Comparative Study of Rotational Bands in the A~60 Mass Region: Modification of Nilsson Parameters

Gellanki, Jnaneswari; Carlsson, Gillis; Ragnarsson, Ingemar; Rudolph, Dirk

Published in:
Physical Review C (Nuclear Physics)

DOI:
10.1103/PhysRevC.89.024301

2014

Comparative study of rotational bands in the $A \approx 60$ mass region: Modification of Nilsson parameters

J. Gellanki,[1] B. G. Carlsson,[2] I. Ragnarsson,[2] and D. Rudolph[1]
[1]*Department of Physics, Lund University, S-22100 Lund, Sweden*
[2]*Division of Mathematical Physics, LTH, Lund University, S-22100 Lund, Sweden*
(Received 15 November 2013; published 3 February 2014)

The large number of high-spin bands that have been observed in $A = 56$–62 nuclei are analyzed systematically within the cranked Nilsson-Strutinsky approach. Optimized Nilsson single-particle parameters are derived from investigations of energy differences between experimental and calculated rotational bands. Specifically, the relative energies of bands in neighboring nuclei whose configurations differ by having a high-j orbital either filled or empty are analyzed. The level schemes calculated with the new Nilsson parameters are compared with those using standard Nilsson parameters. Some configuration assignments are revised.

DOI: 10.1103/PhysRevC.89.024301 PACS number(s): 21.60.Cs, 21.10.Re, 27.40.+z, 27.50.+e

I. INTRODUCTION

A large number of high-spin rotational bands have been identified in the $A = 56$–62 nuclei with $N \geqslant Z$. It is interesting that, starting from the low-spin configurations, one can observe a stepwise evolution when individual particles are excited from the $1f_{7/2}$ shell below the $Z = N = 28$ gap or to the $1g_{9/2}$ shell above the $Z = N = 40$ gap [1]. The corresponding configurations have a larger and larger spin content and become more and more deformed. If the maximum spin in the pure configuration, referred to as $I_{\max}$, is not too large, the rotational band will generally end up in a noncollective state at this spin value, i.e., a terminating band (TB) is formed [2]. However, with more particles excited corresponding to a larger $I_{\max}$, the couplings between the $\mathcal{N}$ shells will prevent termination and the configurations will remain noncollective also for $I = I_{\max}$, so-called nontermination [3]. Indeed, the observed bands that are most deformed are predicted to remain strongly collective in their full spin range up to $I = I_{\max}$.

The highest spin states are observed in ^{62}Zn [1,4] and ^{58}Ni [5,6]. Reaching spins up to $I = 35$ and record-high excitation energies ($E_x > 40$ MeV), the superdeformed (SD) bands in these two isotopes are identified close to $I_{\max}$ or maybe even to $I_{\max}$ for one SD band in ^{62}Zn. Very extensive level schemes have also been deduced for ^{60}Ni [7], ^{59}Cu[8,9], ^{61}Cu [10], and ^{61}Zn [11]. A few bands are seen in ^{56}Ni[12,13], ^{57}Ni [14], ^{59}Ni [15], ^{58}Cu [16,17], and ^{60}Zn [18]. Especially the SD bands in ^{58}Cu and ^{60}Zn are interesting because of their high relative yield and their well-defined configuration assignments [19].

The level schemes in the $A = 60$ region have mainly been analyzed using the cranked Nilsson-Strutinsky (CNS) formalism [2,20,21]. In some cases, also Skyrme Hartree-Fock [16,18,22,23] or relativistic mean-field calculations [19] have been applied, notably even large-scale shell-model calculations [12,24]. In previous papers, the level schemes of the different nuclei have been studied separately, i.e., with no or little comparison with neighboring nuclei. An exception is Ref. [19] where the relative properties of the SD bands in ^{58}Cu, ^{60}Zn and ^{62}Zn were analyzed considering mainly the (effective) alignment of the orbitals which become occupied with increasing mass number. Here we use a similar approach considering firmly established rotational bands in all $A = 56$–62 nuclei. First, the well-defined $1g_{9/2}$ excitations are considered to test that the different assignments are consistent and to possibly infer some reassignments. Then we consider relative excitation energies when a proton or a neutron is added or removed in the intruder $1g_{9/2}$ shell and in the high-$\ell 1f_{7/2}$ shell. The positions of these subshells define the spherical shell gaps for particle numbers 40 and 28, respectively. The comparison of the calculated energies using so-called standard parameters [20] with experiment provides the opportunity to optimize the position of these subshells. Furthermore, from the position of specific high-spin states it is also possible to obtain information of the relative position of the $2p_{3/2}$ and $1f_{5/2}$ shells. It is thus feasible to define improved "new" Nilsson single-particle parameters. The intermediate and high-spin states of the different nuclei are then recalculated using the new parameters. Improvements and differences compared with calculations based on the standard Nilsson parameters are analyzed.

II. THE CRANKED NILSSON-STRUTINSKY FORMALISM

The CNS formalism [2,20,21] is based on the modified oscillator (MO) potential which is cranked around a principal axis. Special methods are introduced to fix configurations based on the occupation of orbitals having their main amplitudes in specific j shells or groups of j shells. In the $A = 60$ region, the active j shells are $1f_{7/2}$, $2p_{3/2}$, and $1f_{5/2}$ in the $\mathcal{N} = 3$ oscillator shell and $1g_{9/2}$ in the $\mathcal{N} = 4$ shell. The $2p_{3/2}$ and $1f_{5/2}$ shells are strongly mixed and treated as one entity labeled as fp, where small contributions from the higher-lying $2p_{1/2}$ shell are also included. With these active subshells, configurations are labeled as

$$[p_1(\pm)p_2, n_1(\pm)n_2] \quad \text{or} \quad [p_1p_2, n_1n_2], \tag{1}$$

where p_1 (n_1) denotes the number of $1f_{7/2}$ proton (neutron) holes and p_2 (n_2) the number of $1g_{9/2}$ protons (neutrons). The number of fp particles is then fixed to get the correct proton and neutron numbers. The "(+)" or "(−)" labels specify the signature of an odd number of protons and neutrons in the fp orbitals, (+) for $\alpha = 1/2$ and (−) for $\alpha = -1/2$. Note also that an odd number of $1g_{9/2}$ protons or neutrons are

assumed to have the favored signature, $\alpha = 1/2$, if nothing else is specified. The (+) and (−) labels are sometimes omitted and never specified for an even number of fp particles which are assumed to have $\alpha = 0$. They were previously introduced in Ref. [1], where they were written in a somewhat different way.

The energies of the different configurations are minimized in the deformation space, ε_2, γ, and ε_4, at each spin value and with respect to all excitations having the same distribution of protons and neutrons over the different groups of orbitals, specified by j shell(s) and signature. Total energies are calculated using the Strutinsky prescription [25,26] as a sum of the shell energy and the rotating liquid drop energy. The latter, $E_{\rm rld}$, is based on the Lublin-Strasbourg drop (LSD) model [27], with the moment of inertia calculated with a diffuse surface [21]. It is then instructive to show the calculated total energies relative to this same rotating liquid drop energy, $E(I) - E_{\rm rld}(I)$, and compare with observed energies. In general, the experimental energies are described with an accuracy of approximately ±1 MeV [21]. However, for a correct description of the quantal shell effects, a smooth variation of the differences between experiment and calculations appears to be more important. In the present work, this variation is tested not only as a function of spin and configuration changes in one specific nucleus, but also for variations of proton and neutron numbers.

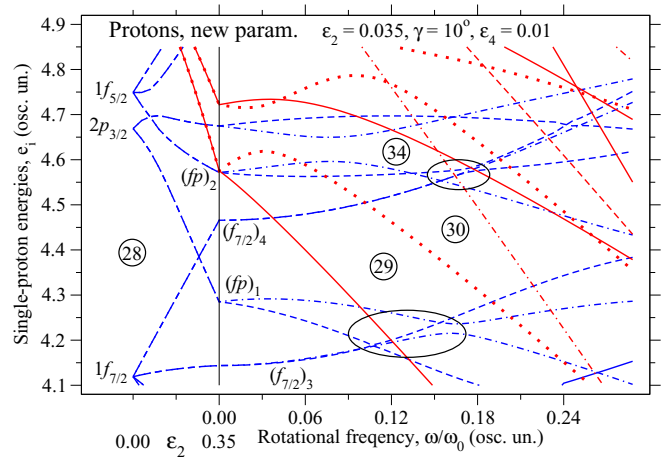

FIG. 1. (Color online) Proton single-particle orbitals at the deformation $\varepsilon_2 = 0.35$, $\gamma = 10^\circ$, and $\varepsilon_4 = 0.01$ drawn as functions of rotational frequency, with the spherical origin of the orbitals traced to the left. The new Nilsson parameters defined in Table III and Fig. 7 have been used. Note the gaps at particle numbers 29 and 30 and the crossings between $1f_{7/2}$ and fp orbitals below and above these gaps. For the region of the (N,Z) chart considered here, these crossings are important for SD bands in nuclei with $Z = 28$ and $N \geqslant 31$, respectively.

A. General features of the configurations in the $A = 60$ region

For a general understanding of the configurations in the $A = 60$ nuclei with their Fermi levels for protons and neutrons just above the $1f_{7/2}$ subshell, one can formulate some specific rules. Similar rules but one $\mathcal{N}$ shell higher up apply to the terminating bands in the $A = 110$ region, as discussed in Ref. [2]. In the $A = 60$ region, general features of the bands can be deduced from the two numbers $[q_1,q_2]$, where $q_1 = p_1 + n_1$ and $q_2 = p_2 + n_2$ [9]. These numbers are useful because the quadrupole deformation ε_2 at low spin is essentially governed by the total number of $1f_{7/2}$ holes and $1g_{9/2}$ particles, i.e., by $q_1 + q_2$. Furthermore, the spin vectors of high-j $1g_{9/2}$ orbitals are easy to align. This leads to a low energy cost of the last spin units before $I_{\rm max}$, leading to so-called favored terminations for large values of q_2. In a favored termination, the $E(I) - E_{\rm rld}(I)$ curve is strongly downsloping, ending in a low-energy noncollective state. On the other hand, holes in the $1f_{7/2}$ shell are difficult to align, which leads to a higher energy cost and thus to more unfavored terminations with increasing values of q_1. An unfavored termination is characterized by a smooth parabolalike $E(I) - E_{\rm rld}(I)$ curve with a positive curvature.

For prolate shape ($\gamma = 0^\circ$), the highest $1f_{7/2}$ orbital has $\Omega = K = 7/2$; i.e., it has the highest possible K value in this mass region. This means that configurations with one proton or one neutron hole in this orbital ($q_1 = 1$) will have two $\Delta I = 2$ partners, one of each signature, which are degenerate; i.e., they follow the same E vs I curve. The degeneracy is understood from the properties of the highest $1f_{7/2}$ orbital labeled as $(1f_{7/2})_4$ in Fig. 1. The bands remain degenerate also for triaxial shape but they might split up close to termination at near-oblate or oblate ($\gamma = 60^\circ$) shape. One may then conclude that configurations of the type $[1p_2,1n_2]$ with one proton and one neutron hole in the highest $1f_{7/2}$ orbital will have four degenerate bands, two of each signature. This is the result without any residual interaction, while in a more complete formalism, the bands having the same signature will interact, leading to one band which is pushed down in energy and another which is pushed up.

B. The limits of the distinction between high-j and low-j orbitals

In the CNS calculations at small and intermediate deformations, a distinction is generally made between low-j and high-j orbitals within the different $\mathcal{N}$ shells. The first case where this feature was explored was for the description of the smooth terminating bands in the $A = 110$ region [28,29]. The TBs in the $A = 60$ region are more or less analogous to those in the $A = 110$ region except that they are formed from orbitals one $\mathcal{N}$ shell further down [2]. Thus, it is important to be able to distinguish between $\mathcal{N} = 3$ orbitals of $1f_{7/2}$ and $1f_{5/2}2p_{3/2}$ character (the fp orbitals), respectively, in the $A = 60$ region in a similar way, as it is important to distinguish between $\mathcal{N} = 4$ proton orbitals of $1g_{9/2}$ and $1g_{7/2}2d_{5/2}$ character in the $A = 110$ region.

The distinction between $1f_{7/2}$ and fp orbitals is rather straightforward for deformations up to $\varepsilon \approx 0.30$ and rotational frequencies that are not too high. However, some of the bands have larger deformations. Then it becomes difficult to fix configurations properly. This is demonstrated by the single-particle orbitals in Fig. 1, which are drawn for protons at a typical deformation for the SD bands in ^{58}Ni or for some of the more deformed bands in ^{62}Zn. Because the proton and neutron orbitals are rather similar, this diagram can be used

also for a general demonstration of the neutron orbitals. In the diagram, the crossings between the highest and next-highest $1f_{7/2}$ orbitals with the $(fp)_2$ and $(fp)_1$ orbitals, respectively, are indicated by ellipsoids. The interaction between the orbitals in these two cases will vary with deformation. In some cases, it will be too strong to be treated as a virtual interaction [20,30,31] and smooth noninteracting orbitals of $1f_{7/2}$ and fp character cannot be formed.

For the crossing between the $(1f_{7/2})_4$ and the $(fp)_2$ orbitals, however, the interaction is never very strong. Therefore, as discussed in Ref. [1], it is possible to force these orbitals to cross at all deformations relevant for the SD bands and thus to form orbitals which are straightforward to use when defining configurations according to Eq. (1).

For the crossing between the $(1f_{7/2})_3$ and $(fp)_1$ orbitals, the interaction strength is sometimes too strong to force the orbitals to cross. Therefore, in the case with one hole in these orbitals, the lowest and next-lowest band is searched [32]. The interaction between these two bands is then "removed," resulting in two noninteracting bands of the character $(1f_{7/2})^{-2}(fp)^1$ and $(1f_{7/2})^{-3}(fp)^2$, respectively, for the $\mathcal{N} = 3$ occupancy. If appropriate, the observed bands are treated in the same way, before comparing with calculations. A crossing of this type is observed in the SD bands in ^{58}Ni [5] and it is also of some relevance in ^{57}Ni; see below.

III. BAND SELECTION

When trying to find improved single-particle parameters for the $A \approx 60$ nuclei, we mainly select those rotational bands in the mass region, which have experimentally well-defined excitation energies, spins, and parities and whose configuration assignments are well established theoretically. However, we also consider a few more bands which are less well established but still interesting, as detailed below. We only consider bands at high spin where pairing correlations are expected to be negligible, say $I \geqslant 15$. In the following, we refer to the experimental bands with their labels defined in the corresponding, original publication. Table I provides a summary of the roughly 50 selected bands, and brief notes follow on each of the isotopes. A more comprehensive assessment is available in Ref. [33].

^{56}Ni. The experimental SD2 band can be described by the calculated band with a [2(+)1,20] configuration. However, exchanging neutrons and protons leads to a band, [20,2(+)1], that has a similar behavior. Therefore, the experimental band can be assigned to any one of these calculated configurations or rather to a mixture of them [34].

^{57}Ni. Band SD1 has been assigned to the [2(+)1,21] configuration. It may gradually change its configuration towards [31,21] at highest spin values; see Ref. [14] and Sec. II B.

^{58}Ni. The bands decaying mainly through quadrupole transitions, Q1a, Q1b, Q2a, Q2b, and Q3, and the three SD structures B1, B2, and B3 (labeled Q4, Q5, and Q6 in Ref. [6]) have been selected. Of the SD bands, only B3 could be assigned to a pure [31,22] configuration, while a crossing between the [31,22] and [21,22] configurations is clearly observed in the B1 and B2 bands; see Ref. [5]. As discussed in Sec. II B, a crossing is "created" between these two bands. The resulting bands are referred to as B1a and B2a. The dipole structures D3a and D3b reach sufficiently high spins and are taken into account as well.

^{59}Ni. Bands 1 and 2 are observed to high-spin values with confirmed spin and parity assignments and they have been assigned to pure theoretical configurations [20,01] and [2(+)1,01], respectively.

^{60}Ni. The M2, WD1a, WD1b, WD2, and WD3 bands are well established experimentally and observed to high-spin values. Thus, even though there are some uncertainties about their configuration assignments (see Table I), they have been selected.

^{58}Cu. The experimentally observed high-spin SD1 band is in near-perfect agreement with the calculated band [21,21].

^{59}Cu. The well-established high-spin bands 5, 6a, 6b, and 8a, 8b have been selected. The high-spin bands 4a, 4b, 7a, 7b, and 10 with uncertain configurations have not been considered.

^{61}Cu. The bands Q4, Q5, Q7, and D3a, D3b are selected because all these are in agreement with CNS calculations. In turn, Q6, Q8, and Q9 are observed with tentative spins only. Therefore, they are neglected.

^{60}Zn. The experimental values for the SD band in ^{60}Zn agrees very well with the calculated [22,22] configuration.

^{61}Zn. Bands SD1, ND5a, and ND5b have been selected. They are well established and in good agreement with the calculated [22,23] configuration and the signature partner bands [11,01], respectively. Despite their tentative connection, the SD bands labeled SD2A, SD2B, and SD2C have been included in Table I. Their absolute excitation energies and their spins are uncertain. However, their relative properties appear to be well established. They have the same parity, and bands SD2A and SD2B are essentially signature degenerate in their full spin range with one $\Delta I = 1$ transition connecting them in both directions. In Ref. [11], these bands were assigned to the [22,12] and [22,22] configurations. We agree on this but differ on details because we assign the two signature partner bands SD2A and SD2B to the [22,12] configuration, where signature-degenerate partners are expected because of the odd neutron in the highest $1f_{7/2}$ orbital. Consequently, SD2C is assigned as [22,22]. These bands are especially interesting because they are closely related to the SD bands of ^{62}Zn.

^{62}Zn. The SD bands SD1, SD2, SD3, and SD5, the well-deformed bands from WD1 to WD7-6, and the normally deformed bands ND3, ND6, ND7, ND8, and ND9 are observed with confirmed spin and parity values and appear to be well understood theoretically. Note, however, that there are some uncertainties about which band should be assigned to which configuration. The bands SD1, SD2, and SD5 have previously been assigned to [22,13]- and [22,23]-type configurations. It is, however, uncertain exactly which configurations should be assigned to which band. One may note that these bands are formed from the [22,12] and [22,22] configurations assigned to the SD2A, SD2B, and SD2C bands in ^{61}Zn by adding a third $1g_{9/2}$ neutron. Therefore, in a way similar to that used with the signature-degenerate bands in ^{61}Zn, SD2A and SD2B, are assigned to the configuration with one $1f_{7/2}$ neutron hole [22,12], the signature-degenerate bands in ^{62}Zn, SD1, and SD2, are assigned to the [22,13] configuration (contrary to the preferred choice in Refs. [1,4]). The SD5 band is then

TABLE I. Rotational bands in the mass $A \sim 60$ region selected to search for improved Nilsson single-particle parameters. Band labels refer to those applied in the original publication.

Nucleus	Bands	$[q_1,q_2]$	Maximum spin, parity, signature	Configuration	Ref.
^{56}Ni	SD2	[4,1]	$I^\pi = 17, \alpha = 1$	[2(+)1,20], [20,2(+)1][a]	[13]
^{57}Ni	SD1	[4,2]	$I^\pi = 47/2^-, \alpha = 1$	[2(+)1,21]	[14]
^{58}Ni	D3a, D3b	[3,1]	$I^\pi = 18^-, 15^-, \alpha = 0, 1$	[20,11]	[5,6]
	Q1a, Q1b	[3,2]	$I^\pi = 22^+, 23^+, \alpha = 0, 1$	[2(+)1,11]	
	Q2a, Q2b	[3,2]	$I^\pi = 20^+, 21^+, \alpha = 0, 1$	[2(−)1,11]	
	Q3	[4,2]	$I^\pi = 22^+, \alpha = 0$	[20,22], [2(+)1,2(+)1][a]	
	B1, B2	[4,3]	$I^\pi = 31^-, \alpha = 1$	[2(+)1,22] [31,22],	
	B3	[5,3]	$I^\pi = 32^-, \alpha = 0$	[31,22]	
^{59}Ni	Band 1	[2,1]	$I^\pi = 37/2^+, \alpha = +1/2$	[20,01]	[15]
	Band 2	[2,2]	$I^\pi = 43/2^-, \alpha = -1/2$	[2(+)1,01]	
^{60}Ni	M2	[1,2]	$I^\pi = 17^+, \alpha = 0, 1$	[11,0(+)1], [1(+)0,02]	[7]
	WD1a, WD1b	[2,1]	$I^\pi = 18^-, 19^-, \alpha = 0, 1$	[20,0(∓)1]	
	WD2	[3,2],[2,3]	$I^\pi = 23^+, \alpha = 1$	[31,0(+)1], [2(+)1,02][c]	
	WD3	[2,2]	$I^\pi = 22^+, \alpha = 0$	[2(+)1,0(+)1], [20,02][b]	
^{58}Cu	SD	[4,2]	$I^\pi = 23^+, \alpha = 1$	[21,21]	[16,17]
^{59}Cu	Band 5	[4,3]	$I^\pi = 57/2^+, \alpha = +1/2$	[21,22]	[8,9]
	6a, 6b	[4,2]	$I^\pi = 49/2^-, 47/2^-, \alpha = +1/2, -1/2$	[21,2(∓)1]	
	8a, 8b	[3,2]	$I^\pi = 47/2^-, 49/2^-, \alpha = -1/2, +1/2$	[21,11]	
^{61}Cu	D3a, D3b	[1,2]	$I^\pi = 37/2^-, 35/2^-, \alpha = +1/2, -1/2$	[1(+)1,0(+)1] [10]	
	Q4	[2,3]	$I^\pi = 53/2^+, \alpha = +1/2$	[21,02]	
	Q5	[4,3]	$I^\pi = 53/2^+, \alpha = +1/2$	[21,22]	
	Q7a, Q7b	[3,3]	$I^\pi = 53/2^+, 55/2^+, \alpha = 1/2, -1/2$	[21,1(∓)2]	
^{60}Zn	SD	[4,4]	$I^\pi = 30^+, \alpha = 0$	[22,22]	[18]
^{61}Zn	SD1	[4,5]	$I^\pi = 57/2^+, \alpha = +1/2$	[22,23]	[11]
	ND5a, ND5b	[1,2]	$I^\pi = 37/2^-, 39/2^-, \alpha = +1/2, -1/2$	[11,01]	
	SD2A, SD2B	[3,4]	$I^\pi = 55/2^-, 57/2^-, \alpha = +1/2, -1/2$	[22,12]	
	SD2C	[4,4]	$I^\pi = 55/2^-, \alpha = -1/2$	[22,2(−)2]	
^{62}Zn	SD1, SD2	[3,5]	$I^\pi = 34^-, 35^-, \alpha = 0, 1$	[22,13]	[1,4]
	SD3	[4,6]	$I^\pi = 30^+, \alpha = 0$	[22,24]	
	SD5	[4,5]	$I^\pi = (29^-), \alpha = 1$	[22,2(+)3]	
	WD1	[2,4]	$I^\pi = 30^+, \alpha = 0$	[22,02]	
	WD2a, WD2b	[2,3]	$I^\pi = 27^-, 28^-, \alpha = 1, 0$	[11,1(+)2]	
	WD3	[2,3]	$I^\pi = 27^-, \alpha = 1$	[22,0(+)1],[2(+)1,02][b]	
	WD4	[1,4]	$I^\pi = 25^+, \alpha = 1$	[1(+)2,02]	
	WD5	[3,4]	$I^\pi = 31^+, \alpha = 1$	[22,1(+)2]	
	WD6-7	[2,3]	$I^\pi = 27^-, \alpha = 1$	[11,1(+)2]	
	WD7-6	[2,3]	$I^\pi = 27^-, \alpha = 1$	[2(+)1,02],[22,0(+)1][b]	
	TB1a, TB1b	[1,2]	$I^\pi = 20^+, 21^+, \alpha = 0, 1$	[11,0(+)1]	
	TB2a, TB2b	[1,3]	$I^\pi = 23^-, 24^-, \alpha = 1, 0$	[11,02]	
	ND9	[0,3]	$I^\pi = 19^-, \alpha = 1$	[0(+)1,02]	
	ND8	[0,2]	$I^\pi = 16^+, \alpha = 0$	[00,02]	
	ND7	[0,2]	$I^\pi = 17^+, \alpha = 1$	[0(+)1,0(−)1]	
	ND6a, ND6b	[0,2]	$I^\pi = 15, 16^+, \alpha = 1, 0$	[0(±)1,0(−)1]	

[a]Possible alternative.
[b]With new parameters these bands are rather assigned to these configurations.
[c]Possible configuration for WD2 with negative parity.

assigned as [22,23], where one notes that the signature of the fp neutrons is different from that of the SD2C band in ^{61}Zn.

IV. EFFECTIVE ALIGNMENTS

In the configuration assignments outlined above, the various nuclei are essentially treated independently. In the following, we test the relative properties of bands in neighboring nuclei, which are identical except that one $1g_{9/2}$ single-particle orbital is either empty or occupied; i.e., the nucleus A converts to $A + 1$ by either an extra neutron or proton $1g_{9/2}$ particle. It is then instructive to introduce the effective alignment $i_{\rm eff}$ [35], which is defined as illustrated in Fig. 2. Thus, $i_{\rm eff}$ is simply the difference in the total spin at a constant frequency, $\hbar\omega = E_\gamma/2$. The values of $i_{\rm eff}$ in the figure illustrate the spin contribution from the second $1g_{9/2}$ neutron and the second $1g_{9/2}$ proton when the SD bands in ^{59}Cu/^{58}Cu and ^{60}Zn/^{59}Cu, respectively,

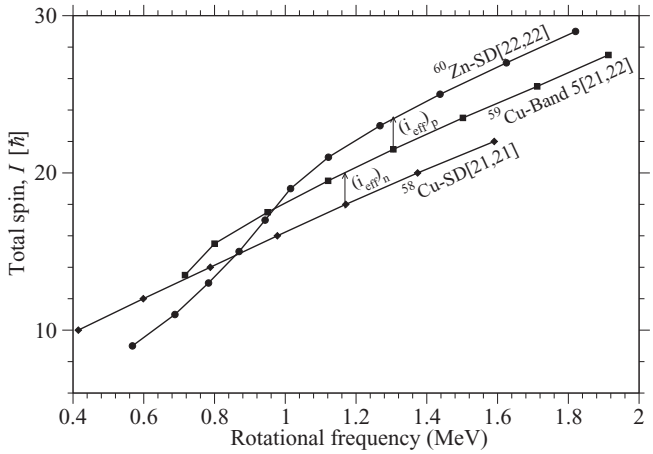

FIG. 2. Total spin vs rotational frequency, $\hbar\omega$ for the SD bands in ^{58}Cu, ^{59}Cu, and ^{60}Zn, illustrating how the effective alignment $i_{\rm eff}$ of the second $1g_{9/2}$ neutron and proton is calculated.

are compared. In this case, for an even-even, odd-even, and an odd-odd nucleus, it is interesting to compare the different I vs ω curves at low spin values, before $i_{\rm eff}$ becomes close to constant for $\hbar\omega > 1.2$ MeV.

The calculated values of $i_{\rm eff}$ should mainly depend on the wave functions of the intruder $1g_{9/2}$ orbitals, which are more or less independent of parameters and therefore yield essentially the same results with any reasonable set of Nilsson parameters.

A. $1g_{9/2}$ neutron alignments

The experimental effective alignments calculated from configurations in neighboring isotopes which are identical but with one extra $1g_{9/2}$ neutron added in the $N+1$ isotope are compared with the N isotope in Fig. 3(a). It is instructive to note the large spin contribution from the first $1g_{9/2}$ particle, the somewhat smaller contribution from the second $1g_{9/2}$ neutron, etc.

The value of $i_{\rm eff}$ for the third $1g_{9/2}$ can be determined either from the well-established SD and SD1 bands in ^{60}Zn and ^{61}Zn, respectively, or from the SD1 and SD2 bands in ^{62}Zn and SD2A and SD2B bands in ^{61}Zn ([22,13] and [22,12] configurations). When calculating $i_{\rm eff}$ in the latter case, the spin values of the SD2A and SD2B bands in ^{61}Zn have been increased by $1\hbar$ compared with the tentative values suggested in Ref. [11]. With this change, the spin contribution from the third $1g_{9/2}$ neutron is very close to identical in the three cases. Therefore, we conclude that the spin values of the SD2A and SD2B bands in ^{61}Zn should indeed be increased by $1\hbar$; i.e., $I^\pi = 35/2^-$ is assigned to the state at the bottom of band SD2A. To make the excitation energy consistent with those observed for the other SD bands in ^{61}Zn and in neighboring nuclei, the energy must be increased by $\approx$2 MeV; i.e., an excitation energy of 15.266 MeV is assumed for this $35/2^-$ state. Because the SD2C band is connected to the SD2B band, the corresponding values for its spin and excitation energies must be modified consistently; i.e., $I^\pi = 31/2^-$ and $E_x = 14.044$ MeV for the lowest state in the band.

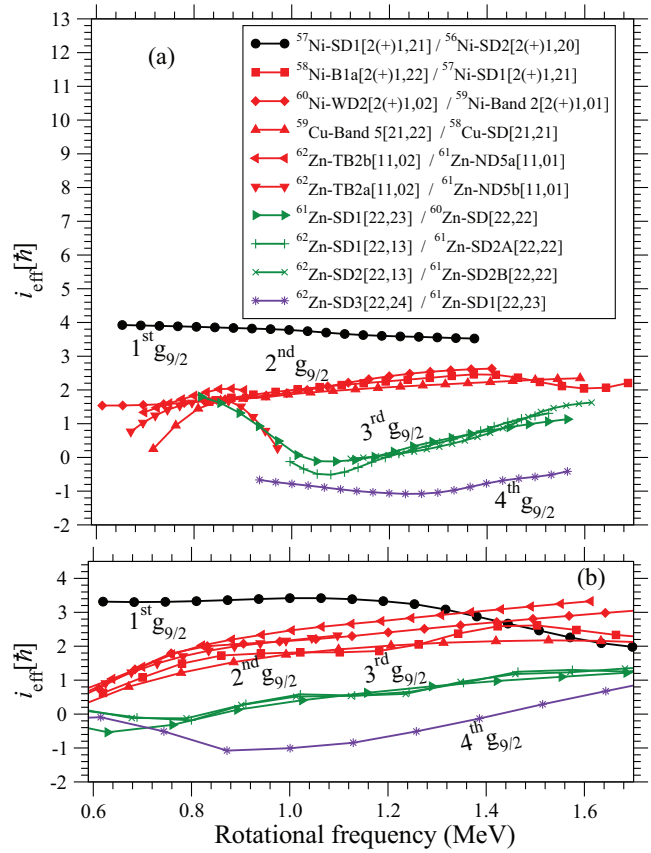

FIG. 3. (Color online) (a) Experimental effective neutron alignments, $i_{\rm eff}$, extracted from various neighboring nuclei in the $A \sim 60$ mass region, which differ by a $1g_{9/2}$ neutron. A spin increment of $1\hbar$ has been applied for the SD2A and SD2B bands in ^{61}Zn (see text for details). Note that for the WD2 band in ^{60}Ni, we have assumed the negative-parity configuration; see Sec. IV C 2. (b) Calculated effective alignments using standard parameters for the configurations assigned to the bands in panel (a).

The calculated values for the spin contribution of $1g_{9/2}$ neutrons for the configurations assigned to the observed bands are shown in Fig. 3(b). The conclusion is that theory and experiment are consistent but with a tendency that the calculated values are somewhat more spread. This can partly be understood from the fact that the common spin interval for some of the observed bands is rather small, and $i_{\rm eff}$ is then drawn in a larger frequency interval for the corresponding calculated bands. Therefore, effects from large shape changes and band terminations will become more important in the calculated bands. Indeed, small discontinuities in the $I_{\rm max} \rightarrow I_{\rm max} - 2$ transition energies leads to large fluctuations in $i_{\rm eff}$ as illustrated in Fig. 1 of Ref. [36]. In view of this, it is gratifying that the values of $i_{\rm eff}$ in Fig. 3 develop so smoothly towards the highest spin values even in the cases when the bands terminate.

It is also instructive to compare the calculated effective alignments with the pure single-particle contributions. At a frequency which depends on the collectivity, the alignment of the lowest orbital in a j shell will approach the maximum value j, the next lowest will approach $j-1$, etc. This is illustrated for a $g_{9/2}$ shell in Ref. [33] and for an $1h_{11/2}$

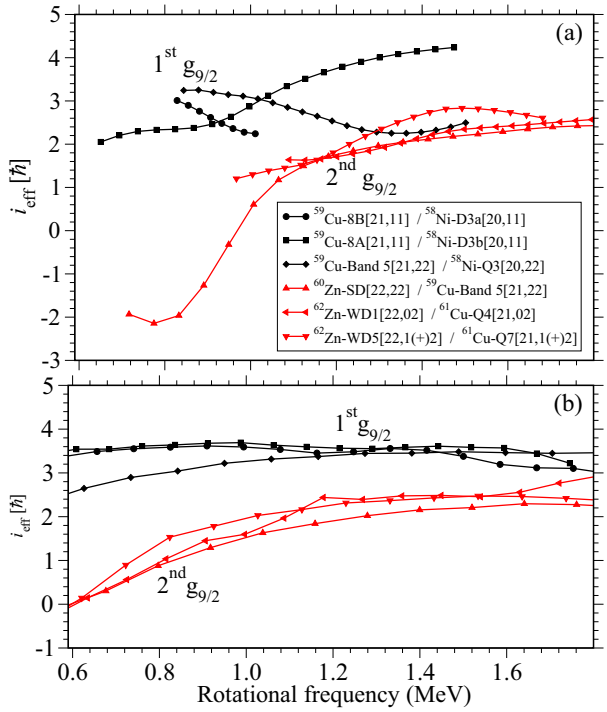

FIG. 4. (Color online) (a) Experimental effective proton alignments, $i_{\rm eff}$, extracted from neighboring nuclei in the $A \sim 60$ region, which differ by a $1g_{9/2}$ proton. (b) Calculated effective alignments using standard parameters for the configurations assigned to the bands in panel (a).

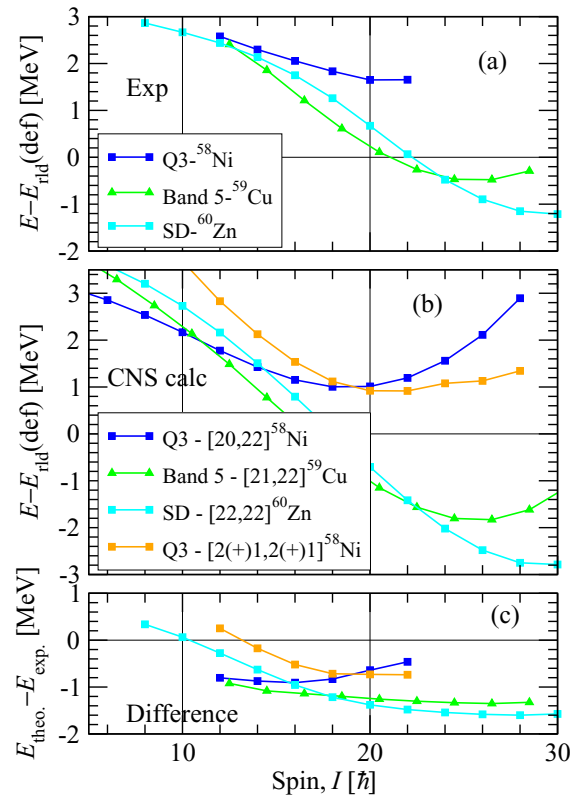

FIG. 5. (Color online) (a) Observed and (b) calculated bands shown relative to the rotating liquid drop energy with the difference between calculations and experiment in panel (c). Two possible assignments for the Q3 band in ^{58}Ni are compared with the well-established assignments for the SD bands in ^{59}Cu and ^{60}Zn. Standard parameters have been used.

shell in Ref. [26]. For SD bands in heavy nuclei, where the shape is relatively stable, the effective alignment comes close to the single-particle alignments, $\langle j_x \rangle$ of the orbital which is occupied and empty, respectively [35,37]. Thus, in this case, the effects from deformation changes are rather small. This is very different for the present bands in the $A = 60$ region, which show pronounced shape changes. Even so, the pure-single-particle alignments are a good first approximation to the $i_{\rm eff}$ values in Fig. 3.

B. $1g_{9/2}$ proton alignments

The $\mathcal{N} = 4$ intruder $1g_{9/2}$ shell is rather pure and similar for protons and neutrons. Thus, one would expect similar values of $i_{\rm eff}$ for the $1g_{9/2}$ proton shell as for the $1g_{9/2}$ neutron shell. This assumption is tested in Fig. 4. The figure shows bands listed in Table I which differ by the occupancy of one $1g_{9/2}$ proton orbital. As no band has more than two $1g_{9/2}$ protons, $i_{\rm eff}$ can only be obtained for the first and second $1g_{9/2}$ orbital. For most of the comparisons, the $i_{\rm eff}$ values above $\hbar\omega = 1$ MeV are very similar for protons and neutrons. Differences at lower rotational frequencies are probably related to variations in pairing strengths at low spins. There is, however, one clear exception, namely the $i_{\rm eff}$ value when comparing band 5 in ^{59}Cu with the Q3 band in ^{58}Ni. Because there is no doubt about the [21,22] assignment for band 5 in ^{59}Cu, the [20,22] assignment for ^{58}Ni band should be reinvestigated; see next section.

C. Reinvestigation of configuration assignments

1. The Q3 band in ^{58}Ni

As mentioned in Sec. IV B, the previously assigned configuration [20,22] [6] for band Q3 in ^{58}Ni is uncertain. Starting from the previous interpretation of band Q3, we relate it to the well-characterized band 5 in ^{59}Cu and the SD band in ^{60}Zn, which have one and two more protons in the $1g_{9/2}$ orbitals, respectively. These three observed bands are shown in the top panel of Fig. 5, while the calculated bands are provided in the middle panel. The difference between calculations and experiment is seen in the bottom panel. With this interpretation, the difference in the bottom panel for the Q3 band has a different trend compared with the other two bands. This suggests some further analysis of the interpretation of the Q3 band in ^{58}Ni. Because of the positive parity, this configuration must have two $1g_{9/2}$ particles. Hence, the only realistic alternative is to consider one $1g_{9/2}$ proton and one $1g_{9/2}$ neutron instead of two $1g_{9/2}$ neutrons. Near-yrast configurations around $I = 20$ have four $1f_{7/2}$ holes. Thus, the [2(+)1,2(+)1] configuration is also drawn in Fig. 5. Based on the differences in the bottom panel, which are more similar to those of the other nuclei, it seems to be the preferred interpretation of the Q3 band. However, the previous [20,22] assignment cannot be ruled out.

2. The WD2 band in ^{60}Ni

The observed band WD2 in ^{60}Ni has been proposed to have positive parity. Based on that, it has been assigned to the [31,0(+)1] configuration [7]. However, as seen in the bottom panel of Fig. 15 in Ref. [7], the difference between calculations and experiment is close to +1 MeV, which is a relatively large value, considering that the difference is rather negative for other similar bands in the region. This puts the assignment in doubt and one might consider other possible interpretations of the WD2 band.

In principle, the directional correlations of oriented states (so-called DCO ratios) listed in Ref. [7] allow for a change of parity of WD2, though it is somewhat puzzling that in that case no decay branches from either WD2 or interconnected 13^- states into any 11^- state in ^{60}Ni were observed in that study. Nevertheless, assuming negative parity, the WD2 band should have three particles in $1g_{9/2}$ orbitals. The best possible assignment is then [2(+)1,02]. It turns out that the difference between calculations and experiment is reduced compared with the [31,0(+)1] assignment. The situation improves further using revised Nilsson parameters (see below).

With a [2(+)1,02] assignment for the WD2 band in ^{60}Ni, one can investigate the effective alignment relative to band 2 in ^{59}Ni, which is assigned as [2(+)1,01]. As seen in Fig. 3, the effective alignment is consistent with the other values obtained for a second $1g_{9/2}$ particle, supporting the revised negative-parity assignment to WD2 in ^{60}Ni.

3. The SD2 band in ^{61}Zn

As discussed in Sec. III, based on the study of effective alignments the spin values of the SD2A, SD2B, and SD2C bands in ^{61}Zn should be increased by $1\hbar$. We thus use these increased spin values in the following and consequently also assume that the bands are 2 MeV higher in energy than the tentative values given in Ref. [11].

V. DETERMINATION OF NEW SINGLE-PARTICLE PARAMETERS

A. Changes in the positions of the j shells

For all selected bands (cf. Table I), CNS calculations with standard parameters were performed. The $\mathcal{N} = 4$, $1g_{9/2}$ and the $\mathcal{N} = 3$, $1f_{7/2}$ orbitals are more pure than the other orbitals ($1f_{5/2}$, $2p_{3/2}$, and $2p_{1/2}$), and the position of the corresponding subshells gives a direct measure of gaps at Z,$N = 28$ and 40. Therefore, we introduce four simple cases, from which one can derive revised energy gaps and thereby determine the new Nilsson parameters:

case 1, addition of a $1g_{9/2}$ neutron particle;

case 2, addition of a $1g_{9/2}$ proton particle;

case 3, creation of a $1f_{7/2}$ neutron hole;

case 4, creation of a $1f_{7/2}$ proton hole.

All these four cases are examined, considering the bands in neighboring nuclei whose configurations are identical except for a particle or hole in the $1g_{9/2}$ or $1f_{7/2}$ orbital, respectively. This comparison is presented in Table II.

Let us exemplify the procedure by looking at band B1a in ^{58}Ni which is assigned to the [2(+)1,22] configuration. The observed and calculated bands are shown relative to the rotating liquid drop energy in Fig. 6 with the difference between experiment and calculations in the bottom panel. In the $I \sim 17\hbar$–$23\hbar$ spin range, the average value of the difference is −0.8 MeV. The SD1 band in ^{57}Ni has the same configuration except for the second $1g_{9/2}$ neutron, i.e., [2(+)1,21]. The difference between calculations and experiment in this case is −1.1 MeV in the same spin range as for the ^{58}Ni band. The spin range is chosen because the ^{57}Ni band is only observed to $I = 47/2\hbar$, while the results become more uncertain for lower spin values where pairing correlations start to become important. The differences for ^{58}Ni and ^{57}Ni, respectively, are listed as $\Delta E_B = -0.8$ MeV and $\Delta E_A = -1.1$ MeV, i.e., $\Delta E_B - \Delta E_A = 0.3$ MeV. We can thus conclude that the differences would be the same if the energy cost when occupying the second $1g_{9/2}$ neutron orbital is 0.3 MeV lower; i.e., this comparison suggests that the $1g_{9/2}$ subshell should be lowered by approximately 0.3 MeV. The same method as for these two bands in ^{57}Ni and ^{58}Ni is now applied to other bands in neighboring nuclei. Table II includes the cases where identical configurations except for one high-j particle are observed in a common high-spin range. Most values for standard parameters in Table II can, in principle, be read out from published $E - E_{\rm rld}$ plots, for example, Refs. [1,4,6,7,10,11,14,15]. Nevertheless, to be consistent we have systematically carried out calculations for all the bands in the table.

In general, the differences $\Delta E_B - \Delta E_A$ using standard parameters in Table II are quite consistent for one specific case. In addition, we have also investigated bands in the same nucleus which differ by an $1f_{7/2} \rightarrow fp$ or an $fp \rightarrow 1g_{9/2}$ excitation as a measure of the position of the $1f_{7/2}$ and $1g_{9/2}$ subshells [33]. These values are more uncertain because they are also sensitive to the position of the fp orbitals. However, they lead to conclusions similar to the cases in Table II.

In Table II, it is found that, using standard parameters, the average energy of the difference $\Delta E_B - \Delta E_A$ for the addition of a $1g_{9/2}$ neutron is +0.5 MeV, for the addition of a $1g_{9/2}$ proton it is −0.7 MeV, for the creation of a $1f_{7/2}$ neutron hole it is −0.3 MeV, and for the creation of a $1f_{7/2}$ proton hole it is −0.1 MeV. A positive value implies that the gaps at particle numbers 40 and 28 should be decreased. Thus, for the $1g_{9/2}$ subshell, positive values indicate that it should be lowered in energy, while positive values for the $1f_{7/2}$ subshell indicates that its energy should be increased. To adjust the differences in Table II towards zero, somewhat larger energy shifts than indicated in the table have to be performed. One can see several reasons for larger shifts:

(i) the $\vec{\ell}_t \cdot \vec{s}$ and ℓ_t^2 terms are generally stronger at spherical than at deformed shapes;
(ii) the shells are not pure at the deformations and rotational frequencies considered;
(iii) the Strutinsky renormalization tends to counteract the shifts.

Note that we use relative energies when fitting the parameters because they are directly related to the position of the j

TABLE II. Comparison of energy differences, $\Delta E = E_{\text{theory}} - E_{\text{exp}}$, between bands of different neighboring nuclei, A and B. The differences, which are illustrated in the bottom panel of Fig. 6, are calculated for four different cases: (1) added $1g_{9/2}$ neutron particle, (2) added $1g_{9/2}$ proton particle, (3) creation of $1f_{7/2}$ neutron hole, (4) creation of $1f_{7/2}$ proton hole. Columns 5 and 6 show results of calculations performed with standard parameters and columns 7 and 8 show results with the new parameters.

	Nuclei	Spin range ($\hbar$)	Band A, Band B	Standard		New	
				Energies ΔE_A, ΔE_B (MeV)	Difference $\Delta E_B - \Delta E_A$ (MeV)	Energies ΔE_A, ΔE_B (MeV)	Difference $\Delta E_B - \Delta E_A$ (MeV)
$\nu(1g_{9/2})$							
	^{57}Ni-^{58}Ni	∼17–23	SD1[21,21] [21,22],B1a	−1.1, −0.8	0.3	−1.2, −1.3	−0.1
	^{58}Cu-^{59}Cu	∼17–23	SD[21,21] [21,22],Band 5	−1.7, −1.3	0.4	−1.35, −1.35	0.0
	^{60}Zn-^{61}Zn	∼22–30	SD[22,22] [22,23],SD1	−1.6, −0.8	0.8	−1.2, −1.2	0.0
	^{61}Zn-^{62}Zn	∼14–20	ND5b[11,01], [11,02]TB2	−0.3, 0.2	0.5	−0.7, −0.6	0.1
		∼22–28	SD1[22,23] [22,24],SD3	−0.8, −0.3	0.5	−0.9, −0.3	0.6
			Avg. diff		0.5		0.1
$\pi(1g_{9/2})$							
	^{58}Ni-^{59}Cu	∼14–18	D3a[20,11] [21,11],8b	0.3, −0.8	−1.1	−0.1, −0.65	−0.55
	^{59}Cu-^{60}Zn	∼22–28	Band 5[21,22] [22,22],SD	−1.3, −1.6	−0.3	−1.5, −1.3	0.2
	^{61}Cu-^{62}Zn	∼20–26	Q4[21,02], [22,02]WD1	0.0, −0.5	−0.5	−1.5,−1.3	0.2
		∼20–27	Q7b[21,1(+)2], [22,1(+)2]WD5	0.0, −1.0	−1.0	−0.6, −0.6	0.0
			Avg. diff		− 0.7		−0.0
$\nu(1f_{7/2})$							
	^{59}Ni-^{58}Ni	∼15–19	Band 1[20,01] [20,11],D3a	0.5, 0.3	−0.2	−0.15, −0.2	−0.05
		∼14–22	Band 2[2(+)1,01], [2(+)1,11]Q1b	0.1, −0.2	−0.3	−0.4, −0.55	−0.15
	^{59}Cu-^{58}Cu	∼16–24	8A[21,11] [21,21],SD	−1.0, −1.4	−0.4	−0.9,−1.3	−0.4
			Avg. diff		−0.3		−0.2
$\pi(1f_{7/2})$							
	^{62}Zn-^{61}Cu	∼18–24	TB2[11,02], [21, 02]Q4	0.1, −0.1	−0.2	−0.7, −0.7	0.0
	^{59}Cu-^{58}Ni	∼22–28	Band 5[21,22] [31,22],B3	−1.3, −1.5	−0.2	−1.5, −1.5	0.0
			Avg. diff		−0.2		0.0

shells. This is contrary to absolute energies which depend on factors that are not well-known, for example the parameters of the rotating liquid drop model. Our procedure to adjust the Nilsson parameters is thus analogous to methods used for SD bands, where it is often advantageous to consider relative properties rather than absolute properties [35,38].

Next to the position of the $1f_{7/2}$ and $1g_{9/2}$ subshells, the relative energies of the $1f_{5/2}$ and $2p_{3/2}$ subshells are also important for the high-spin bands in $A = 56$–62 nuclei, while the $2p_{1/2}$ shell is rather unimportant because it lies at a higher energy, and it can only give marginal contributions to the total spin. As discussed in Ref. [1], the disagreement of the 17^+ and 14^- states of ND7 and ND3b in ^{62}Zn (see the bottom panels of Figs. 22 and 23 in Ref. [1]) suggests that the $1f_{5/2}$ neutron shell should be lowered relative to the $2p_{3/2}$ shell. Furthermore, the wrong signature splitting in the ND4 band in ^{61}Zn [11] suggests a similar lowering of the $1f_{5/2}$ shell for the protons. It appears that a lowering of the $1f_{5/2}$ subshell by approximately 1 MeV ($\sim 0.1\hbar\omega_0$) would cure the problems.

B. New Nilsson parameters for the $\mathcal{N} = 3$ and $\mathcal{N} = 4$ shells

As concluded above, for a better agreement between experimental and calculated energies, it is estimated that the $\mathcal{N} = 4$ proton and neutron $1g_{9/2}$ orbitals should be shifted by a value that is somewhat larger than 0.5 MeV in different directions. After performing some tests, a value of 0.7 MeV, which corresponds to about $0.066\hbar\omega_0$ for the $A \sim 60$ mass region, is found to be appropriate; the neutron $1g_{9/2}$ subshell is shifted downwards while the proton $1g_{9/2}$ subshell is shifted upwards. The energy shifts are obtained by multiplying the κ and μ' parameters by the same factor, which means that the shells are expanded or compressed around their average harmonic oscillator value, $5.5\hbar\omega_0$. The factors which are calculated to get the desired energy shifts of the $\mathcal{N} = 4$, $1g_{9/2}$ neutron and proton subshells are 1.149 and 0.863, respectively, These factors have been used to obtain the new Nilsson parameters specified for the $\mathcal{N} = 4$ shell in Table III.

The analysis of specific states mentioned above indicated that the $1f_{5/2}$ shell should be lowered by ≈1 MeV relative to the $2p_{3/2}$ shell for both protons and neutrons. Furthermore, Table II suggests that the 28 gap should be somewhat larger; i.e., the $1f_{7/2}$ shell should be lowered relative to the $1f_{5/2}$ and $2p_{3/2}$ subshells. Several different tests with ℓ-dependent κ and μ' values have been performed as well, but it was concluded that the desired energy shifts can be obtained simply by changing the strength of the ℓ^2 potential, i.e., the μ' value in the $\mathcal{N} = 3$ shell. Thus, if this value of μ' is increased by 0.01, the $1f$ ($\ell = 3$) shells are lowered by 0.1 $\hbar\omega_0$ (∼1 MeV) relative to the $2p$ ($\ell = 1$) shells. This means that the distance between the $1f_{5/2}$ and the $1f_{7/2}$ shells is not changed while the distance between the $1f_{7/2}$ and the $2p_{3/2}$ shell is increased

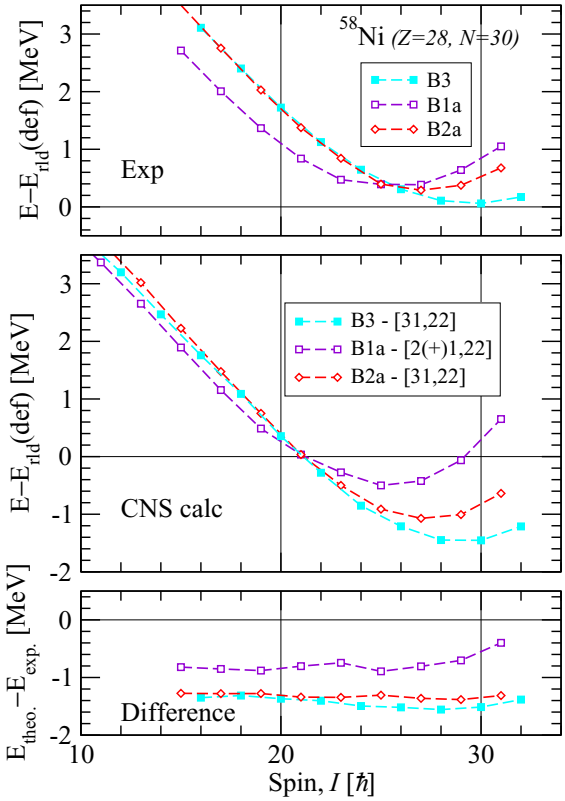

FIG. 6. (Color online) Same as Fig. 5, but for the B1a, B2a (see Sec. III), and B3 bands in ^{58}Ni.

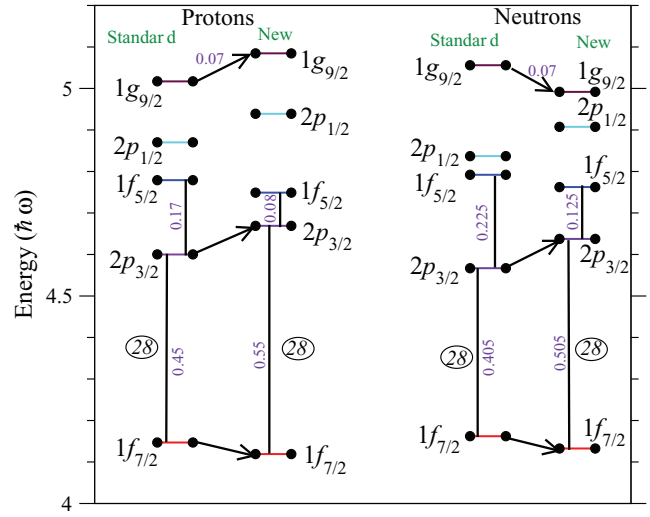

FIG. 7. (Color online) Position of the spherical j shells for standard [20] and new parameters, respectively.

by ∼1 MeV. This corresponds to an effective increase of the 28 gap by ∼0.5 MeV. The resulting values for the κ and μ' parameters for the $\mathcal{N} = 3$ shell are listed in Table III.

The standard and new level energies of $1f_{7/2}$, $1f_{5/2}$, $2p_{3/2}$, and $2p_{1/2}$ from $\mathcal{N} = 3$ and $1g_{9/2}$ from $\mathcal{N} = 4$ shells are shown in Fig. 7. It may appear somewhat surprising that with the new Nilsson parameters the proton $1g_{9/2}$ subshell is placed considerably higher than the $1g_{9/2}$ neutron subshell. This is different from the general understanding in heavier nuclei where the intruder shells are pushed further down for protons than for neutrons. This feature might, however, simply be caused by the excess of neutrons in heavy nuclei. The situation is rather different for the nuclei studied here, which are close to the proton drip line with $N \sim Z$. In any case, the new parameters give an improved description of the $A = 60$ region and provides valuable insight in the structure of the observed bands.

TABLE III. Standard and new Nilsson parameters for $\mathcal{N} = 3$ and $\mathcal{N} = 4$ proton and neutron shells.

		κ_{old}	μ'_{old}	κ_{new}	μ'_{new}
$\mathcal{N} = 3$	Protons	0.090	0.0270	0.090	0.0370
	Neutrons	0.090	0.0225	0.090	0.0325
$\mathcal{N} = 4$	Protons	0.065	0.0370	0.0560	0.0319
	Neutrons	0.070	0.0273	0.0804	0.0313

By using the new Nilsson parameters for the $\mathcal{N} = 3$ and 4 shells listed in Table III, the results using standard parameters are modified as shown in two rightmost columns in Table II. It is evident that the average energy differences for all cases defined in Sec. V A are now close to zero; i.e., the new parameters provide a much improved description of the relative properties of bands with similar configurations in neighboring nuclei.

VI. DISCUSSION

The results with the new parameters are now analyzed for the different nuclei, sometimes comparing with earlier results using the standard parameters. In a few cases the experimental bands have been reassigned to different configurations. A complementary analysis for a few nuclei is presented in Ref. [33].

The general development of the different configurations is rather straightforward. It occurs according to the rules defined in Sec. II A when particles are added or removed from the high-j shells, $1f_{7/2}$ and $1g_{9/2}$. Remember that the parity of the configurations is determined from the number of $1_{9/2}$ particles. Therefore, it is, in general, possible to determine this number, q_2 knowing the parity of a band and the spin range in which it is observed. Then, especially from the properties close to termination and the presence of signature partners, one can often determine the number of $1f_{7/2}$ holes, q_1. Finally, for a complete assignment, the distribution of the particles and the holes over protons and neutrons should be fixed. An instructive example of how these rules can be applied is provided by the very extensive level scheme of ^{62}Zn [1].

A. ^{56}Ni

The two collective bands which have been observed [12,13] in ^{56}Ni have previously been described using the shell model [39], the Skyrme Hartree-Fock method [12], and the present CNS formalism [13,40]. They all give consistent

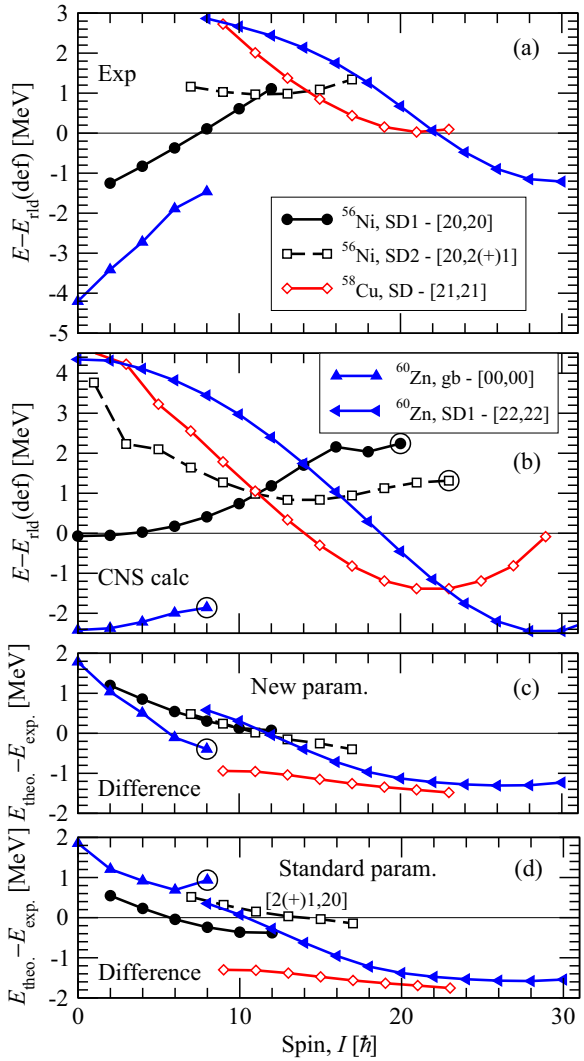

FIG. 8. (Color online) (a) Observed and (b) calculated rotational bands in ^{56}Ni, ^{58}Cu, and ^{60}Zn, shown relative to the rotating liquid drop energy. The difference between calculations and experiment are displayed in panel (c). The new parameters are used in panels (b) and (c). The differences using standard parameters are provided in panel (d) for comparison. Note that the legends applies to the respective observed and calculated bands in all panels.

interpretations with SD1 having four holes in the $1f_{7/2}$ orbitals and four particles in the fp orbitals with one of the fp particles excited to $1g_{9/2}$ in the SD2 band. The agreement between experiment and calculations using new parameters is illustrated in Fig. 8, where also the difference between calculations and experiment using standard parameters is provided. Contrary to most previous calculations, the band with one neutron excited to $1g_{9/2}$ is calculated lower than the band with one proton excited; i.e., it is the [20,2(+)1] configuration that is compared with experiment using the new parameters, while it is the [2(+)1,20] configuration using standard parameters. The experimental band is expected to be a mixture of these two configurations [34]. It is interesting to note that when the configurations of the observed bands are calculated to their I_{max} states, the energy tends to become lower than expected from a smooth interpolation from the lower spin states. As discussed in Ref. [13], these configurations terminate close to spherical shape, where it costs relatively little energy to achieve full alignment of the $1f_{7/2}$ holes.

B. ^{58}Cu

One band which has been referred to as SD has been observed [16] in ^{58}Cu and its transitional quadrupole moment has been measured [17] using DSAM line-shape analysis. It is formed in the $Z = N = 29$ gap in Fig. 1. As seen in Fig. 8, the difference between experiment and calculations is below -1 MeV, but almost constant, showing that the $\mathcal{J}^{(2)}$ moment of inertia is well described by the calculated band. As noticed already in Ref. [17], the transitional quadrupole moment Q_t is somewhat smaller in experiment than in calculations. The measured Q_t decreases slowly with increasing spin, in general agreement with the calculations. This indicates that the SD bands in this region of nuclei tend towards termination when approaching I_{max}, but they are still clearly collective at the $I = I_{max}$ state; cf. Ref. [3].

C. ^{60}Zn

One observed SD band is dominating the level scheme of ^{60}Zn [18]. This band is well described as formed in the $Z = N = 30$ gap in Fig. 1. As seen in Fig. 8, the difference between experiment and calculations comes close to -1 MeV at high spin. In addition to the SD band, also the observed ground band is compared with calculations in Fig. 8. The calculated configuration has the four valence particles in the fp orbitals with $I_{max} = 8$. When comparing the differences between calculations and experiment for new and standard parameters in Fig. 8, it is evident that these difference are somewhat less spread with the new parameters. Furthermore, the large differences with standard parameters at high spin of approximately -1.5 MeV are somewhat reduced with the new parameters. For the new parameters, it appears that the differences come close to -1 MeV when like particle ($T = 1$) pairing is expected to be negligible, i.e., at high spin for the ^{60}Zn SD band, in the full spin range for the doubly odd ^{58}Cu SD band, and at termination of the ground band in ^{60}Zn. One may especially note the large differences between the two parameter sets for the fully aligned $I = 8$ state in ^{60}Zn. The lower value with new parameters is another indication of the improvements resulting from the lowering of the $1f_{5/2}$ subshell.

D. ^{57}Ni

1. The SD bands

The low-spin level scheme of ^{57}Ni has been studied in Ref. [41] and the higher spin states in Ref. [14]. One well-developed band, SD1, is observed in the spin range $I = 27/2$–$47/2^-$. It is well understood as the [2(+)1,21] configuration; see Fig. 9. With the new parameters, it remains "pure" up to its maximum spin, $I = 55/2$, where it is very close to termination.

The interpretation of the second high-spin band, SD2, is more questionable, as discussed in Ref. [14]. An additional

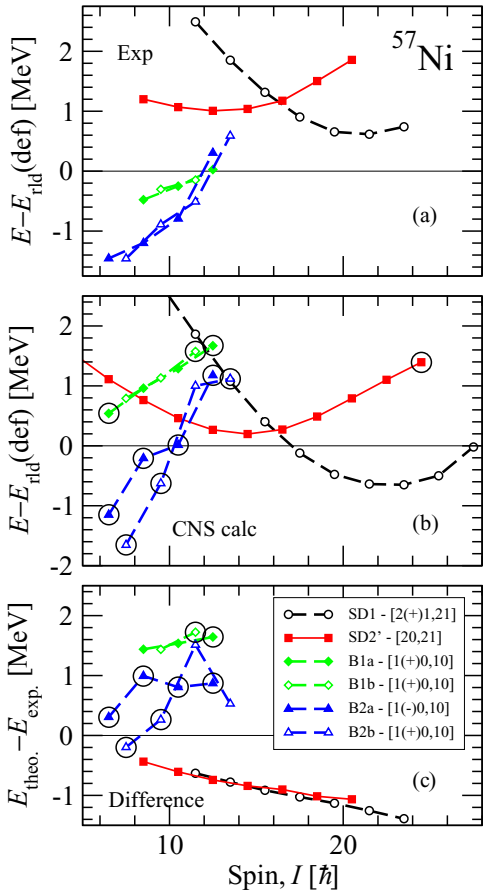

FIG. 9. (Color online) Same as for panels (a)–(c) in Fig. 8, but for ^{57}Ni. See text for the labeling of the observed bands.

problem is that the [2,21] configuration is calculated low in energy but it has no experimental counterpart. One might speculate that the spin values of the SD2 band should be lowered by $2\hbar$, i.e., that the 3349-keV transition links the SD2 state above the 1746 E_γ ray into band B1. Because of the 1746/1745-keV doublet in the SD2 and B1 bands, this is consistent with the coincidence relationships seen in Figs. 2(d) and 2(e) of Ref. [14]. However, it leads to some difficulties concerning the intensities of the respective transitions. In any case, with this assumption and with the SD2 band (labeled SD2′ in Fig. 9) assigned to the low-lying [2,21] configuration, the differences between experiment and calculations are very much in line with the differences seen for the SD1 band and for similar bands in neighboring nuclei.

2. *The bands observed in the $I < 15$ spin range*

It is instructive to consider some of the bands which are seen at lower spin values, i.e., the band B1 shown in Ref. [14] and also the band which ends at tentative $25/2^-$ and $27/2^-$ states at 11.248 and 12.545 MeV [14,41]. We refer to this band as B2. Both these bands, which are shown in panel (a) of Fig. 9, have two branches, a and b, connected by $M1$ transitions. Because of this and because of their spin range, they must be assigned to configurations with one $1f_{7/2}$ hole for both protons and neutrons [10,10], or $\pi(1f_{7/2})^{-1}(fp)^1\nu(1f_{7/2})^{-1}(fp)^2$. Combining the two signatures of the proton and neutron $(1f_{7/2})$ holes and the fp proton, there are, in total, eight "bands" of this kind. However, because of the small deformation, the the two signature partners formed by a hole in the $(1f_{7/2})$ subshell are not degenerate, contrary to collective, and close to prolate configurations, whose properties are outlined in Sec. II A.

Band B2 is considerably lower in energy than B1 at low spin, consistent with the fact that two of the calculated bands are clearly lower in energy than the other six bands. The lowest band is essentially formed from noncollective rotation around the prolate symmetry axis ($\gamma = -120^\circ$) with band heads formed at $I = 13/2,15/2$ with the two $1f_{7/2}$ holes fully aligned combined with an fp proton with a spin projection of $\pm 1/2$, i.e., $I = 7/2 + 7/2 \pm 1/2$. The two signatures are thus formed from the fp proton while the $(1f_{7/2})^7$ proton and neutron structures have a fixed signature of $\alpha = -1/2$ throughout the band. The highest possible spin in this configuration is $I_{max} = 7/2 + 7/2 + 5/2 + 4 = 27/2$, which corresponds to the tentatively observed highest spin state in the band [41]. This description of the bandheads and highest spin states appears consistent with the shell-model calculations of Ref. [41]. Then it is probably a questionable approximation to assume that the intermediate spin states are formed from rotation around one principal axis so it is not so strange that the differences between calculated and observed energies are somewhat scattered.

The band B1 is then assigned to a more standard high-K structure which is essentially prolate at intermediate spin values and terminates at oblate shape for $I = 25/2$. The two signatures are formed from the $1f_{7/2}$ proton hole ([303] 7/2 Nilsson orbital at prolate shape) while the the fp proton and the $1f_{7/2}$ neutrons both have a fixed signature of $\alpha = 1/2$. This leads to a maximum spin state of $I = 7/2 + 5/2 + 5/2 + 4 = 25/2$, which agrees with the highest observed spin state of B1. Comparing observed and calculated energies in Fig. 9, one should note that there are several [10,10] bands, not shown in the figure, that are calculated at similar energies as the [1(+)0,10] bands in Fig. 9. These bands are expected to mix with a resulting band somewhat lower in energy.

E. ^{58}Ni

Many high-spin bands of different character have been observed in ^{58}Ni [5,6]. There are two dipole bands, D2 and D3, in the spin range $I = 10$–18, three quadrupole bands, Q1–Q3, for $I = 12$–23, where signature-degenerate partners are observed for Q1 and Q2. Finally, there are three more quadrupole bands, B1–B3 (Q4–Q6 in Ref. [5]), which are observed beyond $I = 30$. Comparisons with CNS calculations were previously presented using parameters with an enlarged $Z = 28$ gap for the three high-spin bands in Ref. [5] and for the other bands using standard parameters in Ref. [6]. From Fig. 10 one notes that essentially all differences are close to constant as functions of spin, which gives a high confidence for the different assignments. Furthermore, with the increased $Z = 28$ gap for the new parameters, the differences for the three high-spin bands are almost identical. However, they have rather large negative values below -1 MeV.

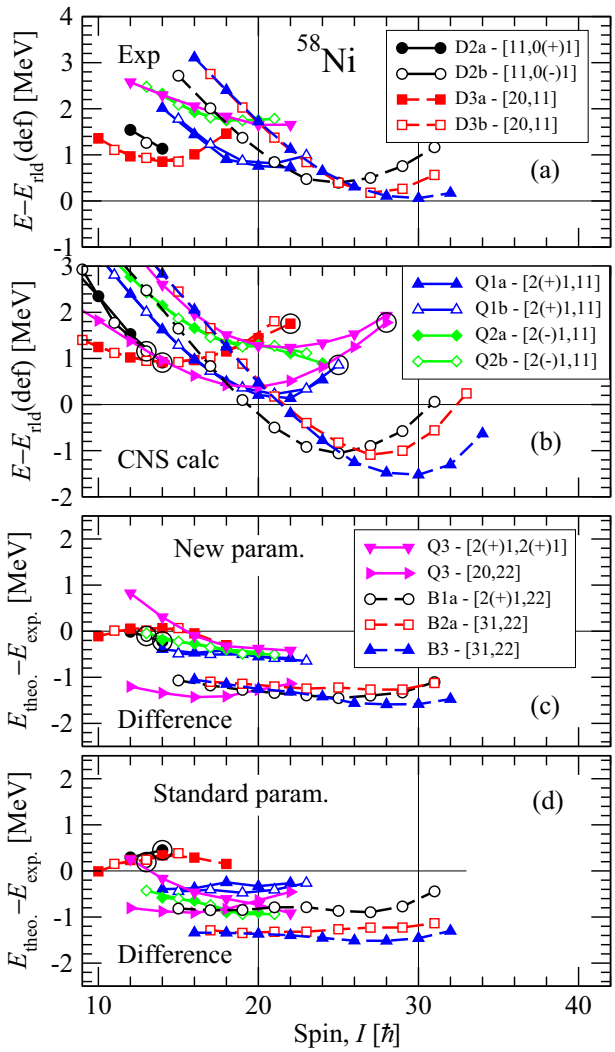

FIG. 10. (Color online) Same as Fig. 8, but for ^{58}Ni. Compared with Ref. [6], some lower spin states down to the 14^+ state at 15.010 MeV have been identified in the Q1 band. Furthermore, the Q3 band is compared with two different CNS configurations. The crossing between the B1 and the B2 bands has been removed so that two smooth noninteracting smooth bands, B1a and B2a, are formed which can be assigned to specific CNS configurations; cf. Sec. II A and Ref. [5].

Furthermore, it is satisfying that with the possible exception of the [2,22] configuration (see below), the configurations that are calculated low in energy are assigned to observed structures.

There are some uncertainties for the Q3 band. Using effective alignments, it was concluded above that the [2,22] assignment from Ref. [6] is somewhat problematic and that [2(+)1,2(+)1] might be a better alternative. In general, with this assignment, the difference between experiment and calculations is more in line with that for the other bands in the same spin range. However, with the new parameters, this configuration is calculated high above the [2,22] configuration so one would rather expect to observe this latter configuration. In conclusion, the Q3 band is assigned to a $[q_1,q_2] = [4,2]$ configuration, but it remains unclear how the $1g_{9/2}$ particles should be distributed over protons and neutrons.

Together with ^{62}Zn, the high-spin bands in ^{58}Ni are observed to higher frequencies than any other bands in the $A = 60$ region. It is then interesting to note that the bands in ^{58}Ni are well reproduced also at the highest spin values while there appear to be some problems at the highest frequencies for the ^{62}Zn bands (see below).

F. ^{59}Ni

Four collective high-spin bands in the approximate spin range $I = 10$–25 have been observed in ^{59}Ni [15]. The bands B1 and B2 have preliminary links to the lower spin states, while B3 and B4 are unlinked. The bands were compared with CNS calculations in Ref. [15], where the configurations assigned to them support the tentative spin values for the linked bands and suggest spin values also for the unconnected bands.

In the present calculations, where, contrary to Ref. [15], also absolute energies are considered, these assignments are supported and strengthened; see Fig. 11. Thus, the [20,01] and [2(+)1,01] configurations assigned to the B1 and B2 bands are clearly the lowest energy calculated bands in the $I = 10$–20 spin range. The unlinked band B3 is then assigned to the signature partner of the B2 band, [2(−)1,01]. With this interpretation all these three bands are observed to their I_{max} values where it is questionable if the I_{max} state is noncollective or not as discussed in Ref. [15]; see also Ref. [3]. Even though the high energy of the highest spin state in band B1 is only partly reproduced by the calculations (see Fig. 11), this high energy is a strong indication that the configuration has indeed reached its I_{max} value. Compared with the B2 and B3 bands, the configuration assigned to the unlinked B4 band, [2(+)1,12], has one more neutron excited from $1f_{7/2}$ to $1g_{9/2}$. The comparison suggests that this band is observed two transitions short of the I_{max} value which equals 57/2. This configuration has a signature-degenerate partner which has not been observed.

Transitional quadrupole moments have been extracted for the bands B1 and B2. The present calculations support previous conclusions that the calculated values are somewhat smaller than the measured ones, while the decreasing trend with increasing spin is reproduced.

G. ^{60}Ni

In ^{60}Ni it appears possible to follow the observed [7] structures from the ground band to the highest spin band through stepwise excitations from the $1f_{7/2}$ shell to the fp orbitals and from the fp orbitals to the $1g_{9/2}$ shell. The comparison with calculations is provided in Fig. 12. With the new parameters, the differences between experiment and calculations follow a smooth trend with values close to zero for spin values $I > 10\hbar$. The trends are similar with standard parameters, but the values are considerably more scattered.

1. The bands with zero or one $1f_{7/2}$ hole

The ground band is seen to the maximum spin in the $\nu(fp)^4$ configuration, $I = 6$. Then the first excitation is when one

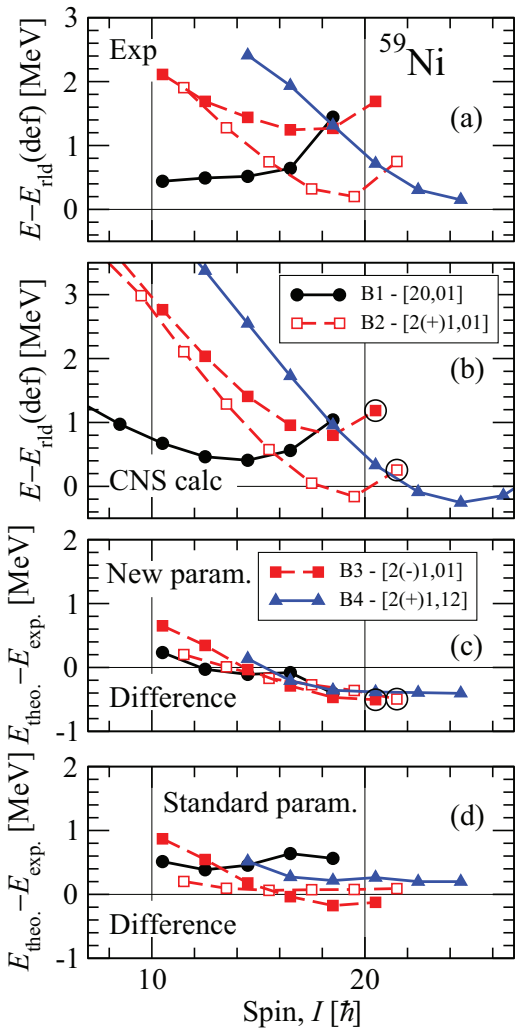

FIG. 11. (Color online) Same as Fig. 8, but for the high-spin bands in ^{59}Ni. The spin values and excitation energies for the unlinked bands B3 and B4 have been chosen so that the differences between experiment and calculations show similar trends for all the bands; $I_0 = 21/2$ with an excitation energy of $E_0 = 9.8$ MeV (new parameters) or 9.3 MeV (standard parameters) for band B3 and $I_0 = 29/2$ with $E_0 = 13.8$ MeV (both parameter sets) for B4.

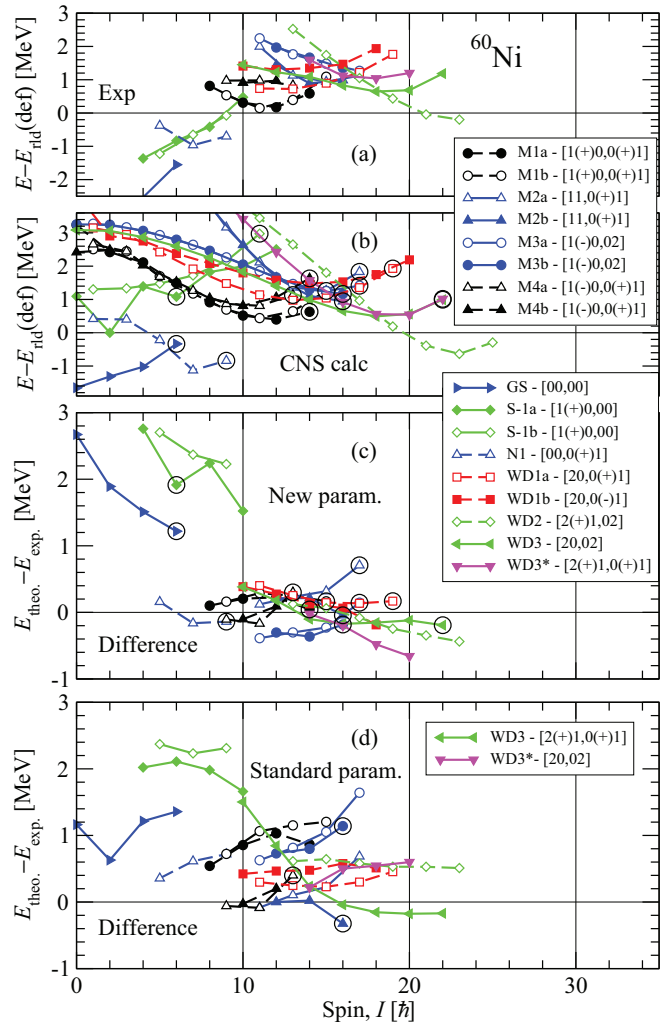

FIG. 12. (Color online) Same as Fig. 8, but for ^{60}Ni. In the comparison with new parameters, WD3 has been assigned to the [20,02] configuration and WD3′ to [2(+)1,0(+)1]. These assignments are reversed for standard parameters as specified in the legend in the bottom panel. Note that the scale is expanded in panels (c) and (d).

proton is excited from $1f_{7/2}$ to the fp orbitals, resulting in the S-1 band, which is compared with the lowest minimum of the [1(+)0,00] configuration in Fig. 12. There is also a [1(−)0,00] configuration at similar energies but independent of interpretation, this low-spin band is not well described in the CNS formalism. The lowest negative-parity configuration with a 5^- at 5.014 MeV, 7^- at 5.349 MeV, and 9^- at 6.811 MeV was not discussed in Ref. [7]. It is labeled N1 in Fig. 12 and well described by the configuration with one neutron excited to $1g_{9/2}$, [00,0(+)1].

The general features of the negative-parity dipole bands in the $I = 8$–15 spin range, M1 and M4, are well described by the two lowest [10, 01] configurations while another particle has been excited to the $1g_{9/2}$ subshell for the positive-parity dipole bands in the spin range $I = 11$–17, M2 and M3. Considering mainly the curvatures of the bands, we assign the M2 band to the lowest [11,01] configuration and the M3 band to the lowest [10, 02] configuration, even though, with new parameters, the differences between experiment and calculations would come somewhat closer to zero if these assignments were reversed. Furthermore, if the 17^- state of the M2 band were assigned to the [11,0(−)1] configuration instead, the large discrepancy between experiment and calculations seen for this state would be removed.

2. *The well-deformed bands*

The interpretation of the well-deformed (WD) bands is rather interesting. The two WD1 branches of negative parity must be assigned to configurations with only one $1g_{9/2}$ particle but with two $1f_{7/2}$ holes to provide high-enough spin values. The only possibility is the [20,0(±)1] configurations, which nicely reproduce the observed band.

It was discussed in Sec. IV C 2 that the parity of the WD2 band is very likely negative, contrary to the choice in Ref. [7]. The band is then well reproduced by the [2(+)1,02] configuration. If the parity is positive instead, this band must be assigned to the [31,01] configuration. With the new parameters, this assignment leads to large differences between experiment and calculations, strongly supporting the conclusion that the parity of the WD2 band is indeed negative.

The WD3 band has positive parity and is observed up to $I = 22$, which means that it has two $1f_{7/2}$ holes and two $1g_{9/2}$ particles, $[q_1,q_2] = [2,2]$. With standard parameters, the lowest such configuration is [2(+)1,0(+)1], which was assigned to the WD3 band in Ref. [7]. However, with such an interpretation, the differences between experiment and calculations become large at lower spin values. These differences become smaller with a [20,02] interpretation. Indeed, from single-particle Routhians drawn as a function of rotational frequency, it is easy to conclude that the spin dependence will be different for a $\nu(1g_{9/2})^2$ configuration compared to a $\pi(1g_{9/2})\nu(1g_{9/2})$ configuration.

With the new parameters, the [2(+)1,0(+)1] and [20,02] bands are calculated as almost degenerate for the highest spin values, $I = 20$ and 22. Thus, the [20,02] band is predicted much lower in energy at lower spin values in close agreement with the observed WD3 band. Consequently, the WD3 band is assigned to a [20,02] configuration, instead of the [2(+)1,0(+)1] assignment made in Ref. [7].

There is also a sideband to WD3 with tentative spin and parity assignments which is labeled as WD3* in Fig. 12. This sideband is compared with the [2(+)1,0(+)1] configuration using new parameters in Figs. 12(b) and 12(c), but such an interpretation is tentative. In Fig. 12(d), WD3 is compared with the [2(+)1,0(+)1] and WD3* with the [2, 02] configuration.

H. ^{59}Cu

A large number of bands has been observed in ^{59}Cu [9]. Most of them have been assigned to specific CNS configurations. This includes bands 5, 6, and 8 listed in Table I and, in addition, bands 4 and 7, which are understood as having one proton and one neutron hole in $1f_{7/2}$ orbitals. For the configurations assigned to both band 4 and band 7, four close-to-signature-degenerate bands are calculated, while only two bands are observed; see Sec. II A. According to the present comparison (see Fig. 13 and Ref. [9]), the interpretation of these five bands in terms of CNS configurations is very well understood with no reasonable alternative assignments.

Band 4 is assigned to the [10,11] configuration. The two signatures of the $1f_{7/2}$ proton and neutron hole result in four calculated bands with $I_{\max} = 35/2^+,37/2^+,37/2^+$, and $39/2^+$. However, an $I = 41/2$ state has been observed, which appears to belong to the band. The two bands with $I_{\max} = 37/2^+$ are calculated degenerate in energy in their full spin range (see Sec. II A), while the band with $I_{\max} = 39/2^+$ comes slightly below the band with $I_{\max} = 35/2^+$ at high spin. The calculated bands do not become fully noncollective when they reach their respective $I_{\max}$ states. Indeed, they can be followed beyond $I_{\max}$, as demonstrated in Fig. 13, where the $41/2^+$ state is shown for one of the bands with $I_{\max} = 37/2^+$.

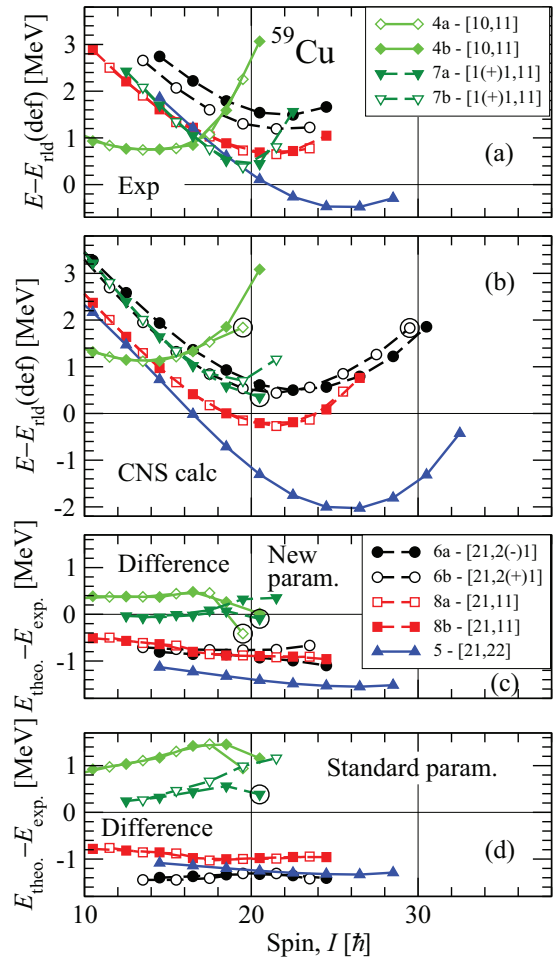

FIG. 13. (Color online) Same as Fig. 8, but for ^{59}Cu. Note that one branch of the [10,11] configuration, which is assigned to band 4, is followed $2\hbar$ beyond its $I_{\max}$ value.

In addition, the signature branch with $I_{\max} = 39/2^+$ is shown in Fig. 13. The fact that the $41/2^+$ state is observed close to where it is predicted supports the present interpretation. To our knowledge, this is the first case where evidence has been presented that any rotational band can be followed beyond its $I_{\max}$ state.

Band 7 is observed to a tentative $45/2^-$ state corresponding to the $I_{\max}$ value in the configuration assigned to it, [1(+)1,11]. In Fig. 13, the two branches, 7a and 7b, are compared with the lowest calculated bands of the type [1(+)1,11] with $I_{\max} = 41/2$ and $43/2$, respectively. The aligned $I_{\max} = 45/2$ state with both the $1f_{7/2}$ holes in the $m_i = -7/2$ state is not shown in Fig. 13(b). It is, however, calculated at a relatively high energy in agreement with the observed $45/2$ state shown in Fig. 13(a) (see also Ref. [9]). As discussed in Sec. II A, the two CNS configurations which can be assigned to each of the branches of bands 4 and 7 are expected to mix, resulting in one band somewhat lower in energy. It is the lower one of these mixed bands that should be compared with experiment, leading to somewhat lower values for the difference curves of these two bands in Fig. 13.

The other bands shown in Fig. 13 have straightforward interpretations and are well described in the sense that the differences between experiment and calculations are almost constant in each case. However, these differences have rather large values, especially for band 5, but it follows the trend from similar high-spin bands in the neighboring nuclei. With new parameters, the differences for all the bands are reasonably well collected while they are more spread with standard parameters.

I. ^{61}Cu

Observed [10] and calculated states in ^{61}Cu are compared in Fig. 14. The figure includes all bands with fixed spins and excitation energies according to Figs. 17 and 18 in Ref. [10], where the assignments are summarized in Table 4. In addition, the Q0 structure (see the caption of Fig. 14) assigned to the favored [01, 01] configuration has been included. We have also found that spin values and excitation energies can be chosen such that the unlinked bands QXa and QY are rather well described as signature partners of the [21,1(−)2] configuration.

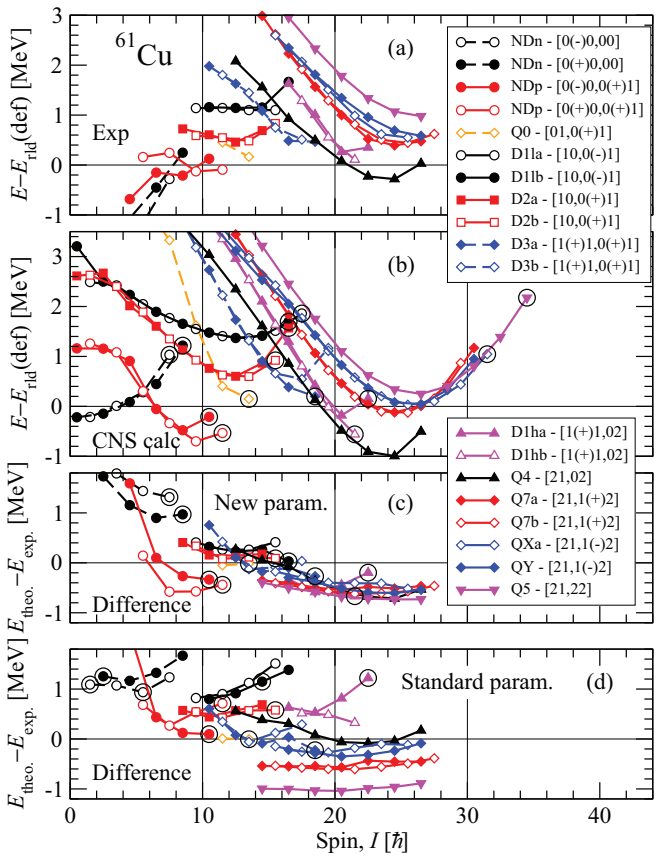

FIG. 14. (Color online) Same as Fig. 8, but for ^{61}Cu. The bands are labeled as in Ref. [10], but with some modifications. The two ND structures are labeled by parity, NDp ($\pi = +$) and NDn ($\pi = -$), respectively. Furthermore, we have followed the convention from other nuclei and labeled the two signature branches as a and b. Therefore, the two structures labeled D1a and D1b in Ref. [10] are labeled D1l (low spin) and D1h (high spin) instead. We have added the structure Q0, which is built from the $23/2^-$ state at 7937 keV and the $27/2^-$ state at 9408 keV. The bottom of the QY band fed by the 1846-keV transition is assumed to have $I = 33/2^+$ at an excitation energy $Y = 14.7$ MeV, and for the bottom of the QX band fed by the 1699-keV transition, $I = 31/2^+$ and $X = 13.4$ MeV. The corresponding band is labeled QXb; i.e., the energy at the bottom of the QXa band ($I = 33/2^+$), which is fed by a 1730-keV transition, is 13.852 MeV.

With the new parameters, the differences in Fig. 14 are well collected and they follow the expected trend, being essentially constant in the high spin range and then increasing gradually towards lower spin values, where pairing correlations are expected to become more important. Note that all high-spin bands are built from the proton '[21,' configuration corresponding to the $Z = 29$ gap in Fig. 1, combined with neutron configurations where two of the five orbitals above the $Z = 30$ gap (see Fig. 1) are occupied. These types of $N = 32$ neutron configurations have previously been discussed for ^{62}Zn; see Refs. [1,4] and below.

Let us also briefly discuss the bands with tentative spin assignments which are shown in Fig. 19 of Ref. [10], but not included in Fig. 14. With the new parameters, the Q6 band is rather well described by the [21,11] configuration. The differences between experiment and calculations are very close to constant but at a value which is somewhat higher than the trend in Fig. 14, namely at ∼0.5 MeV. For the Q8 band, the [21,0(+)1] configuration leads to differences around −0.6 MeV, in close agreement with the trend in Fig. 14.

There remain some unsettled issues, however. Thus, for the Q9 band, the present calculations using new parameters support the conclusions in Ref. [10] that it is not possible to find any reasonable configuration assignment. Furthermore, because the QXa and QXb bands are linked, the excitation energy and spin values of the QXb band is fixed if the values of the QXa band are chosen as in Fig. 14. However, with these values, we have not found any reasonable assignment for the QYb band, which puts some doubt on the interpretation of the QXa band and then also on the suggested signature partner band, QY.

J. ^{61}Zn

The ^{61}Zn nucleus was studied in Ref. [11], where the different bands were interpreted in the CNS formalism. The observed and calculated bands are compared using the new parameters in Fig. 15. Starting from the ground band ND1 with all valence particles in the fp orbitals, downsloping bands are created; first ND2 with one particle excited to $1g_{9/2}$ and then ND4 with two particles excited to $1g_{9/2}$. In the next step, the addition of holes in $1f_{7/2}$ makes the bands less favored in energy at termination: ND5 with one such hole and ND8 and ND9 with two holes. A possible configuration for the latter bands is [2(+)1,01] or, alternatively, one of the [11,1(+)1] and [11,1(−)1] configurations. For these latter configurations, one would then expect the two bands with the same signature to interact, forming one mixed band at a somewhat lower energy. The relative energies and curvatures of the [11,1(+)1] and [11,1(−)1] configurations agree rather well with those of the ND9 and ND8 bands, so that is our preferred assignment. One

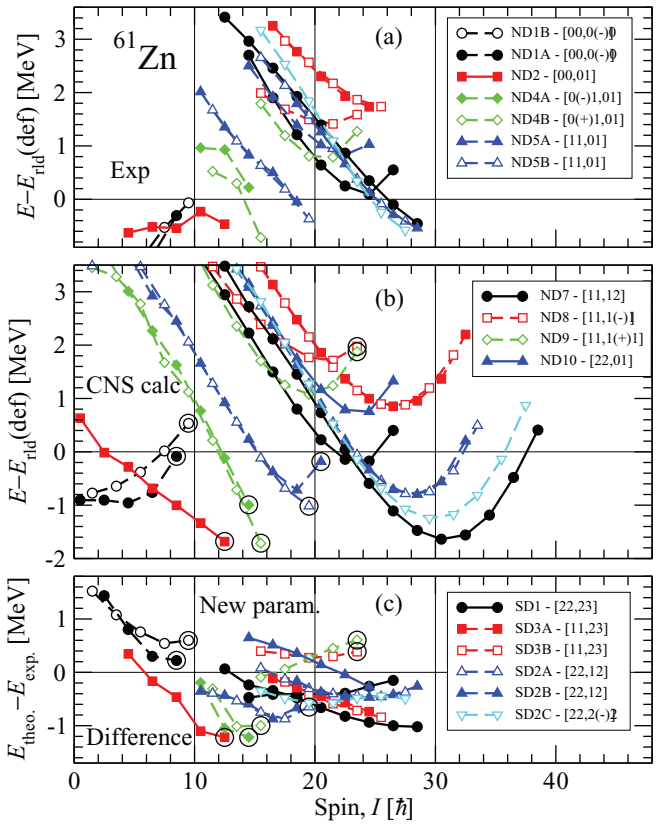

FIG. 15. (Color online) Same as Figs. 8(a)–8(c), but for ^{61}Zn.

could especially note that the lowering of the $1f_{5/2}$ orbital lowers the energy close to termination for the [11,1(−)1] configuration, leading to an improved agreement when this configuration is assigned to the ND8 band. The ND8 band was assigned to a configuration with one more $1f_{7/2}$ hole in Ref. [11] but with the increased $Z = 28$ gap; this configuration, [2(−)1,1(−)1] comes at a higher energy and is not a probable candidate. However, the [2(+)1,01] configuration is clearly an alternative assignment for the ND9 band.

With one more $1g_{9/2}$ particle, the lowest configurations are the four [12,13] bands and the [22,01] band. They have $E - E_{\rm rld}$ curves with minima around $I = 24$ with shapes which are very similar to those of the ND7 and ND10 bands. The comparison between calculations and experiment suggests that ND7 should be assigned as [11,12] and ND10 as [22,01]. The latter configuration is somewhat interesting because it is obtained from the highly symmetric [22,02] configuration assigned to the WD1 band in ^{62}Zn by removing the second $1g_{9/2}$ neutron. There is one further problem with the present assignments, namely that the parity of band ND10 is not established experimentally [11]. However, the suggested positive parity is supported by the fact that no low-lying band with a minimum in the $E - E_{\rm rld}$ curve close to $I = 24$ is calculated for the negative-parity configurations, i.e., for the configurations with an even number of $1g_{9/2}$ particles.

Continuing to higher spin values, we find the negative-parity configurations SD2A, SD2B and SD2C and SD3A, and SD3b. Their $E - E_{\rm rld}$ curves have their minima at $I = 26$–30, if the spin values and energies of the SD2 bands are increased by $1\hbar$ and 2 MeV, respectively, compared with the values used in Ref. [11]; see Sec. IV C 3. The calculated lowest energy negative-parity configurations which have their minima in this spin range are [22,12] and [22,2(±)2]. Thus, SD2A and SD2B are assigned to the signature partners [22,12] and SD2C to [22,2(−)2], which is calculated lower in energy than [22,2(+)2]. The next-lowest calculated bands with four $1g_{9/2}$ particles are [11,23] and [2(±)1,23] which come at a similar energy but where the signature degeneracy and the $M1$ transitions at the bottom makes [11,23] the preferred assignment for the SD3 bands. This leads to a nice agreement between experiment and calculations, which is also the case for the SD1 band of positive parity which is clearly assigned to the [22,23] configuration.

Note that the $f_{5/2}$ proton orbital was lowered in energy because of the signature splitting in the ND4 band and with the new parameters, this splitting is roughly reproduced by calculations. Furthermore, with standard parameters the highest spin state in the ND1 band with a $(1f_{5/2})^2(2p_{3/2})^1$ neutron configuration is calculated much too high in energy but with the new parameters, the difference curve continues smoothly to this state with $I = 19/2^-$.

At superdeformation several bands are built from the proton configuration corresponding to the $Z = 30$ gap in Fig. 1. Except for the rather high-lying [22,01] configuration, this gap is combined with neutron configurations corresponding to this same gap plus one particle in the orbitals just above the gap, namely the two signatures of the highest $1f_{7/2}$ orbital leading to the [22,12] configurations, the two signatures of the second fp orbital ([22,2(±)2] configurations), and finally the third $1g_{9/2}$ orbital ([22,23] configuration). According to Fig. 15, four of these five configurations have been observed.

K. ^{62}Zn

It was in ^{62}Zn that the first SD band in the $A = 60$ region was identified [42]. The high-spin bands in ^{62}Zn were extensively discussed in Ref. [1]. The different structures are naturally grouped according to the number of $1g_{9/2}$ particles, q_2, because the spin values where the configurations come down into the yrast region are strongly correlated to q_2. The classification becomes rather straightforward because, with no excitations outside the $\mathcal{N} = 3,4$ valence space, even (odd) values of q_2 correspond to positive- (negative-) parity states.

1. *Structures assigned to configurations with zero or two* $1g_{9/2}$ *particles*

The positive-parity bands are compared to the configurations assigned to them in Fig. 16. The ground band is assigned to the [00, 00] configurations and the ND6 and ND7 bands are assigned to [01, 01] configurations, where the general agreement between calculations and experiment is very good for the lowest band, ND6. The highest spin in [01, 01] configurations, the 17^+ state of band ND7, has a well-defined interpretation. It is therefore important that it is much better reproduced with the lowering of the $1f_{5/2}$ subshell. In the configuration assigned to the 15^+ state of ND7 in Fig. 16, the 15^+ state is also calculated as aligned. Therefore, it is not so strange that the relative energies of the 15^+ and 17^+ states of

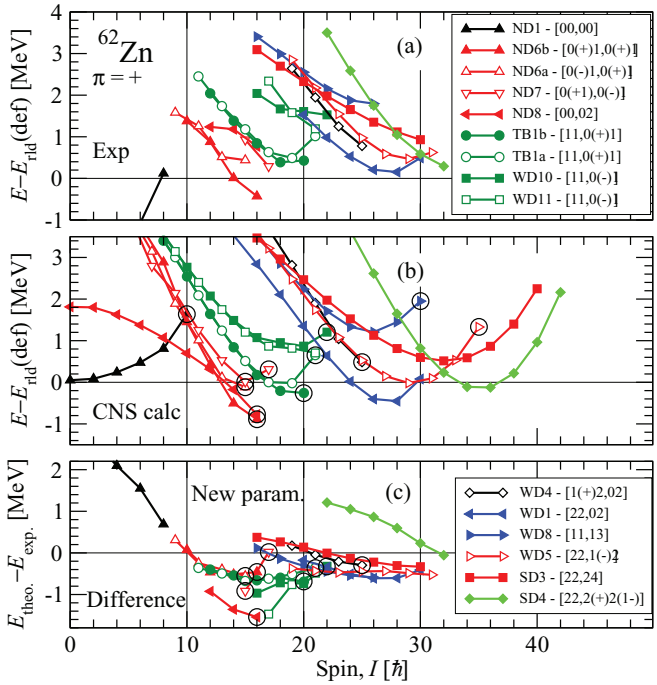

FIG. 16. (Color online) Same as Figs. 8(a)–8(c), but for positive-parity bands in ^{62}Zn.

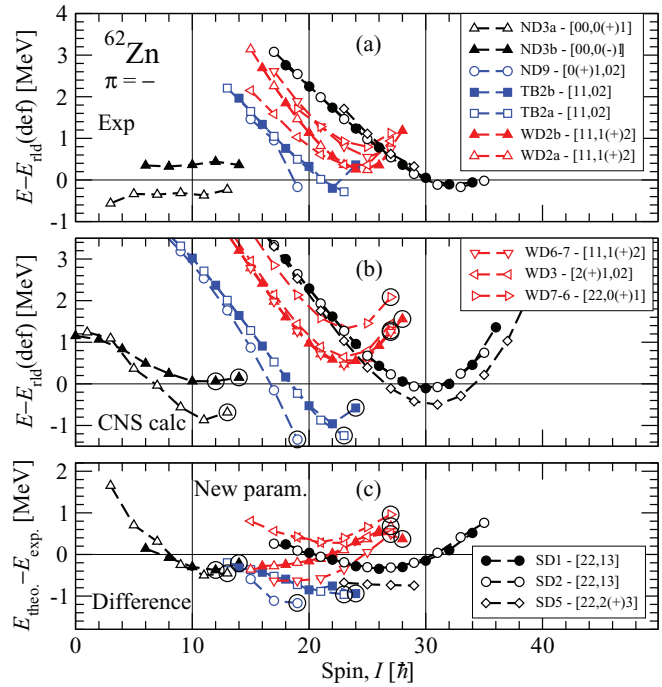

FIG. 17. (Color online) Same as Figs. 8(a)–8(c), but for negative-parity bands in ^{62}Zn.

ND7 are not reproduced by the present assignments, because there is no clear band structure below the 17^+ state. One could imagine that ND8 should be assigned as a signature partner of ND7, but this signature partner is calculated higher in energy and it appears much more plausible that it should be assigned to the [00, 02] configuration, which is calculated much lower in energy.

The TB1 band is well described by the [11,0(−)1] configuration, as noticed long ago [43]. Then, however, the WD10 band is clearly best described by the same configuration, but with signature $\alpha = 1/2$ for the fp neutrons. With the new parameters, this configuration, [11,0(+)1], is calculated around 1 MeV below [2(+)1,0(+)1], which was assigned to WD10 in Ref. [1]. WD10 is observed to $I = 22^+$, which is the highest possible spin in [11,01] configurations. This fact that WD10 terminates makes the observed unsmooth energies more plausible. In Fig. 16 it is also suggested that the WD11 band is a signature partner of WD10, which seems plausible for the $I = 19,21$ but not really for the $I = 17$ state.

2. *Structures with four or six* $1g_{9/2}$ *particles*

Positive-parity bands with higher spin are assigned to the same configurations as in Ref. [1]. It is gratifying that all the calculated low-lying positive-parity configurations up to $I \approx 30$ are assigned to observed bands. At higher spin, there are four [22,12] and one [22,22] configurations that come very close in energy and where only one [22,1(−)2] is assigned to an observed band, WD5. In Ref. [1], WD5 was assigned to a [22,1(+)2] configuration instead, which is calculated very close in energy. The assignment of WD8 remains tentative while the assignment for SD3 with six $1g_{9/2}$ particles is well motivated. Finally, the $E - E_{\rm rld}$ curve of the SD4 band is strongly downsloping at $I = 30$, indicating that it might have a neutron excited to $1h_{11/2}$, but as seen in Fig. 16, the lowest calculated band of this type is even more downsloping, making the evidence for an $1h_{11/2}$ excitation tentative.

3. *Structures with one or three* $1g_{9/2}$ *particles*

The observed and calculated negative-parity states of ^{62}Zn are compared in Fig. 17. For the low-spin states including the TB2 band, there are no decisive differences compared with Ref. [1], though the highest spin state in the ND3b band is now well reproduced, while it is 1 MeV off with standard parameters [1]. As for the positive-parity case, the low-spin configurations calculated low in energy are observed.

There are five observed negative-parity bands with their $E - E_{\rm rld}$ minima around $I = 25$. They have similar curvatures with somewhat higher excitation energies than most of the other observed bands. Their general properties are well understood from the configurations with two $1f_{7/2}$ holes and three $1g_{9/2}$ particles, $[q_1,q_2] = [2,3]$. Possible assignments are eight [11,12] configurations which come in two groups of four signature-degenerate bands. Two [21,02] and two [22,01] configurations are predicted close in energy. The signature-degenerate WD2 bands are naturally assigned to the lowest [11,1(+)2] bands, while the assignment of the other three observed signature $\alpha = -1/2$ bands is more uncertain. The assignments of WD3, WD6-7, and WD7-6 are in line with those in Ref. [1], except for an interchange of the configurations assigned to WD3 and WD6-7 whose relative energies become reversed with the new parameters.

4. *Structures with five* $1g_{9/2}$ *particles*

The negative-parity SD1, SD2, and SD5 bands must be assigned to configurations with two $1g_{9/2}$ protons and three $1g_{9/2}$ neutrons. They are formed in the $Z = 30$ deformed gap, i.e., with two $1f_{7/2}$ proton holes. With the new parameters, the neutron configurations with one and two $1f_{7/2}$ holes come rather close in energy. Thus, as discussed above, we have assigned the SD1 and SD2 bands to the signature-degenerate [22,13] configurations and SD5 as [22,2(+)3]. This leads to absolute differences between experiment and calculations well within the range of ± 1 MeV. Even so, these assignments are somewhat problematic. Thus, for the SD1 and SD2 bands, there is a strong upslope in the differences in the bottom panel of Fig. 16; i.e., the difference at the minimum for $I \approx 26$ is around -0.3 MeV, while it is 0.75 MeV at the highest spin state, $I = 35$. This indicates that it is energetically too expensive to build the highest spin states. As seen in Fig. 17, the shape of the $E - E_{\rm rld}$ curve for the [22,2(+)3]configuration is almost identical to that of the [22,13] configurations, so the problems would remain if the SD1 and SD2 bands were assigned to the [22,23] configurations instead. In general, it is energetically cheaper to build the high-spin states with more high-spin particles, which explains why, before the parity was measured [22,24], was selected as the most likely assignment for the SD1 band in Ref. [19].

Another problem with the present assignments for the SD bands is that the [22,23] configurations are calculated lowest in energy for $I \approx 30$, but the [22,2(+)3] configuration is only observed in a short spin range below $I = 30$ and the predicted lowest-energy configuration, [22,2(−)3], is not observed at all. Thus, it seems that the clarification of the SD bands in ^{62}Zn and their interpretation is a challenge for future investigations of the high-spin bands in the $A = 60$ region.

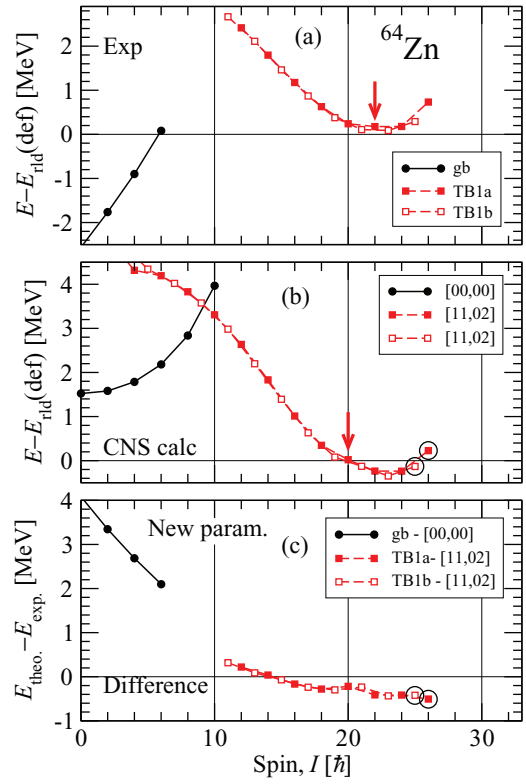

FIG. 18. (Color online) (a) The observed ground band and TB1 band in ^{64}Zn and (b) the calculated configurations assigned to these bands are shown relative to the rotating liquid drop energy, with the difference between calculations and experiment shown in panel (c). The new parameters have been used. The legends apply to the respective panels. Note the band crossings indicated by arrows for the observed even spin states around $I = 22$ and in both signatures of the calculated bands around $I = 20$.

L. The terminating band in ^{64}Zn

It was in ^{64}Zn that the first rotational band in the $A = 60$ region was identified [44,45] and interpreted as a smooth TB with one proton hole in the $1f_{7/2}$ orbitals. Subsequently, the band was linked and observed to termination at $I = 26$ in Ref. [32]. A small discontinuity in the band could be reproduced as a crossing between two fp neutron orbitals by lowering the $1f_{5/2}$ subshell by approximately 300 keV relative to the $2p_{3/2}$ subshell. With the present new parameters, the $1f_{5/2}$ subshell is lowered even more, which means that the crossing is calculated at a slightly too-low spin value. This is indicated in Fig. 18, where the band is labeled TB1. This band is analogous to the TB2 band in ^{62}Zn but with two extra fp neutrons, which give a spin contribution of $2\hbar$ at termination. In addition to TB1, another collective band has been observed in the $I \sim 15$–23 spin range, but it is not firmly linked and has no obvious interpretation; see Ref. [32].

M. The three unlinked high-spin bands in ^{65}Zn

None of the three high-spin bands observed in ^{65}Zn are linked. However, from comparisons with calculations and with the linked TB1 band in ^{64}Zn, it appears possible to fix the spin values and then also to get a good estimate of the excitation energy, say within ± 0.5 MeV.

The three high-spin bands were investigated and interpreted using Hartree-Fock calculations in Ref. [23]. We agree with that reference about which are the important configurations. However, we disagree on some specific assignments. Thus, from the fact that two of the bands, B2 and B3, have signature-degenerate partners, we conclude that they must have one hole in the highest $1f_{7/2}$ orbital with the Nilsson label [303] 7/2 at prolate shape. Thus, the similarities with the linked TB in ^{64}Zn can be explored. This band in ^{64}Zn has the configuration [11,02], which implies that the low-lying ^{65}Zn configurations with a signature-degenerate partner will have the additional neutron in either the fp or the $1g_{9/2}$ orbitals, i.e., [11,02] or [11,03]. The fact that B1 is the most collective band suggests that it has another $1f_{7/2}$ proton hole, where the [22,03] configuration is clearly most favored as also concluded in Ref. [23]. We thus arrive at the comparison between calculations and experiment according to Fig. 19, where the spin values have been chosen so that the difference curves between experiment and calculations are close to zero and similar to those for ^{64}Zn.

The spin values for all three bands appear to be pretty well established. Thus, because Band 1 is assigned to a

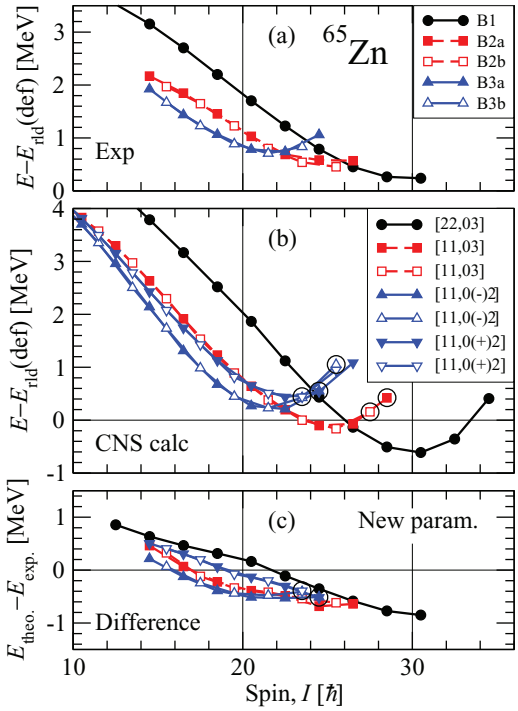

FIG. 19. (Color online) Same as Fig. 18, but for ^{65}Zn. Note that band B3 is compared with two configurations which differ in the signature of the fp neutrons.

configuration with signature $\alpha = 1/2$, its spin value can only be changed in steps $\Delta I = 2\hbar$. However, such a large change leads to unrealistic slopes in the difference curve in the bottom panel. Because of the two signature-degenerate partners in Band 2, its spin values can be changed in steps of $\Delta I = 1\hbar$, accompanied by an interchange of the configurations assigned to the two bands. However, band B2 has the same configuration as the TB1 band in ^{64}Zn except for an added $1g_{9/2}$ neutron. We can thus compare the effective alignment of this third $1g_{9/2}$ neutron with that of the well-established cases discussed in Sec. IV A. Such a comparison is provided in Fig. 20. It is seen that the contribution from the $1g_{9/2}$ neutron in ^{65}Zn is somewhat larger but still similar to that from the third $1g_{9/2}$ neutron in the SD1 band of ^{61}Zn. This somewhat larger value can be understood from the faster alignments of the $1g_{9/2}$ neutrons at the smaller deformation of the ^{64,65}Zn bands, as can be seen, e.g., from diagrams in Ref. [33]. Nevertheless, a lowering of the spin value by $1\hbar$ for band B2 in ^{65}Zn is not excluded from these values of $i_{\rm eff}$.

The assigned signatures for the B2 bands is supported by the dynamical moments of inertia $\mathcal{J}^{(2)}$ of the observed bands, shown in Fig. 21. The crossing between fp orbitals resulting in the bump in $\mathcal{J}^{(2)}$ for the TB1a band in ^{64}Zn was discussed above. The difference between the two bands in ^{64}Zn must be caused by somewhat different deformations when the proton hole is in one or the other signature of the $1f_{7/2}$ orbital. It is now evident (see Fig. 21) that also in the B2a band in ^{65}Zn, one can see the beginning of such a bump but not in the B2b band. It is thus proposed that those bands in ^{64,65}Zn with similar $\mathcal{J}^{(2)}$ have the proton hole in the same orbital. This is consistent with the spin values chosen in Fig. 20.

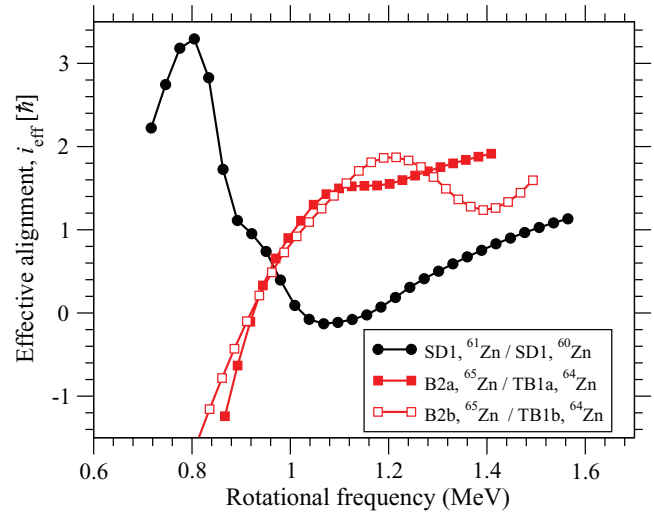

FIG. 20. (Color online) Experimental effective alignments, $i_{\rm eff}$, extracted for the third $1g_{9/2}$ neutron from SD bands in ^{61,60}Zn and from TB bands in ^{65,64}Zn, respectively.

The B3 band in ^{65}Zn is well described by a [11,02] configuration. However, there are two such pairs of bands with a different signature of the third fp proton. Because they are calculated at a similar energy (see Fig. 19) it is not possible to determine which of them should be assigned to the observed band B3.

VII. SUMMARY AND CONCLUSIONS

High-spin rotational bands in $A = 60$ nuclei have been systematically analyzed with CNS calculations. Based on a comparison of related bands in neighboring nuclei, we have derived new Nilsson single-particle parameters which give an improved overall description of the data. Especially, the relative errors comparing experiment and calculations are, in general, much smaller.

Our analysis has led to some reassignments of configurations. Thus, for ^{57}Ni, we have concluded that if the spin values of the SD2 band are decreased by $2\hbar$, it agrees nicely with the

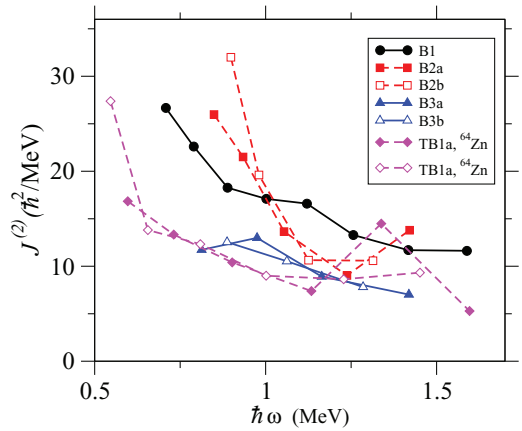

FIG. 21. (Color online) The $\mathcal{J}^{(2)}$ moments of inertia for the observed high-spin bands in ^{65}Zn compared to those for the TBs in ^{64}Zn.

highly symmetric $\pi(1f_{7/2})^{-2}(fp)^2\nu(1f_{7/2})^{-2}(fp)^2(1g_{9/2})^1$ configuration. In ^{60}Ni, there are strong arguments that the parity of the observed WD2 band is negative, contrary to the preferred choice in Ref. [7]. Furthermore, it appears that the WD3 band should be assigned to a configuration with two $1g_{9/2}$ neutrons instead of one $1g_{9/2}$ neutron and one $1g_{9/2}$ proton, supporting the conclusion that the $1g_{9/2}$ proton subshell is higher in energy than the $1g_{9/2}$ neutron subshell.

By comparing the bands in ^{61}Zn and ^{62}Zn, it is concluded that the spin values of the three SD2 bands in ^{61}Zn should probably be increased by $1\hbar$. In ^{62}Zn, the TB1 and TB2 bands have long been well established [43], while the WD1 band was discovered more recently. These three structures have unique interpretations, with one and two proton holes, respectively, in the $1f_{7/2}$ subshell. From comparisons with the WD1 band, some reassignments were suggested in ^{61}Zn. Furthermore, in ^{62}Zn with the new parameters, one of the less well-established bands, WD10, may be assigned to the [11,0(−)1] configuration, i.e., the $\nu(fp)$ signature partner of the [11,0(+)1] configuration assigned to the TB1 band.

The intense SD bands in ^{58}Cu, ^{59}Cu, and ^{60}Zn are interesting because they are built in the large single-particle gaps for particle numbers 29 and 30, which show up at large deformation and large rotational frequencies. However, they are all calculated more than 1 MeV too low in energy and this is true also for the related highest spin bands in ^{58}Ni. Going to somewhat heavier nuclei, the differences between experiment and calculations are generally smaller. This is true also for the SD bands in ^{62}Zn, which have been observed up to very high spins. A major problem in ^{62}Zn, however, is the spin dependence, where the calculated bands are clearly too high in energy at the highest spin values. Another problem is that the SD configuration which is calculated lowest in energy in ^{62}Zn has no experimental counterpart.

The high-spin bands in the $A = 60$ region have mainly been interpreted using CNS calculations based on the MO potential. It would be interesting to compare with calculations based on some finite-depth potential like Woods-Saxon and Folded-Yukawa and, of course, to carry out more extensive calculations using density functional theory approaches, eventually guided by CNS band assignments. On the experimental side, it seems most important to try to settle remaining questions concerning the SD bands in ^{62}Zn. This requires more extensive studies at the highest possible spins or, alternatively, pushing the experimental bands in the neighboring nuclei ^{61}Zn or ^{61}Cu up to similar rotational frequencies as achieved in ^{62}Zn. Another challenge would be to verify that one band in ^{59}Cu is indeed observed one transition beyond the $I_{\max}$ value, $37/2^+$, of the configuration assigned to the band.

ACKNOWLEDGMENT

This work was supported by the Swedish Research Council.

[1] J. Gellanki *et al.*, Phys. Rev. C **86**, 034304 (2012).
[2] A. V. Afanasjev, D. B. Fossan, G. J. Lane, and I. Ragnarsson, Phys. Rep. **322**, 1 (1999).
[3] J. J. Valiente-Dobón *et al.*, Phys. Rev. Lett. **95**, 232501 (2005).
[4] J. Gellanki *et al.*, Phys. Rev. C **80**, 051304(R) (2009).
[5] D. Rudolph *et al.*, Phys. Rev. Lett **96**, 092501 (2006).
[6] E. K. Johansson *et al.*, Phys. Rev. C **80**, 014321 (2009).
[7] D. A. Torres *et al.*, Phys. Rev. C **78**, 054318 (2008).
[8] C. Andreoiu *et al.*, Phys. Rev. C **62**, 051301(R) (2000).
[9] C. Andreoiu *et al.*, Eur. Phys. J. A **14**, 317 (2002).
[10] L.-L. Andersson *et al.*, Eur. Phys. J. A **36**, 251 (2008).
[11] L.-L. Andersson *et al.*, Phys. Rev. C **79**, 024312 (2009).
[12] D. Rudolph *et al.*, Phys. Rev. Lett. **82**, 3763 (1999).
[13] E. K. Johansson *et al.*, Phys. Rev. C **77**, 064316 (2008).
[14] D. Rudolph *et al.*, J. Phys. G **37**, 075105 (2010).
[15] C.-H. Yu *et al.*, Phys. Rev. C **65**, 061302(R) (2002).
[16] D. Rudolph *et al.*, Phys. Rev. Lett. **80**, 3018 (1998).
[17] D. Rudolph *et al.*, Phys. Rev. C **63**, 021301(R) (2000).
[18] C. E. Svensson *et al.*, Phys. Rev. Lett. **82**, 3400 (1999).
[19] A. V. Afanasjev, I. Ragnarsson, and P. Ring, Phys. Rev. C **59**, 3166 (1999).
[20] T. Bengtsson and I. Ragnarsson, Nucl. Phys. A **436**, 14 (1985).
[21] B. G. Carlsson and I. Ragnarsson, Phys. Rev. C **74**, 011302(R) (2006).
[22] C.-H. Yu *et al.*, Phys. Rev. C **60**, 031305(R) (1999).
[23] C.-H. Yu *et al.*, Phys. Rev. C **62**, 041301(R) (2000).
[24] M. Horoi, B. A. Brown, T. Otsuka, M. Honma, and T. Mizusaki, Phys. Rev. C **73**, 061305(R) (2006).
[25] V. M. Strutinsky, Nucl. Phys. A **95**, 420 (1967).
[26] G. Andersson *et al.*, Nucl. Phys. A **268**, 205 (1976).
[27] K. Pomorski and J. Dudek, Phys. Rev. C **67**, 044316 (2003).
[28] I. Ragnarsson, V. P. Janzen, D. B. Fossan, N. C. Schmeing, and R. Wadsworth, Phys. Rev. Lett **74**, 3935 (1995).
[29] A. V. Afanasjev and I. Ragnarsson, Nucl. Phys. A **591**, 387 (1995).
[30] I. Hamamoto, Nucl. Phys. A **271**, 15 (1976).
[31] T. Bengtsson, Nucl. Phys. A **496**, 56 (1989).
[32] D. Karlgren *et al.*, Phys. Rev. C **69**, 034330 (2004).
[33] J. Gellanki, Ph.D. thesis, Lund University, 2013, http://lup.lub.lu.se/record/3971316.
[34] W. Satula, J. Dobaczewski, W. Nazarewicz, and M. Rafalski, Phys. Rev. C **81**, 054310 (2010).
[35] I. Ragnarsson, Nucl. Phys. A **557**, 167 (1993).
[36] A. V. Afanasjev and I. Ragnarsson, Nucl. Phys. A **628**, 580 (1998).
[37] I. Ragnarsson, Nucl. Phys. A **520**, 67c (1990).
[38] B. R. Mottelson, Nucl. Phys. A **557**, 717 (1993).
[39] T. Mizusaki, T. Otsuka, M. Honma, and B. A. Brown, Nucl. Phys. **704**, 190c (2002).
[40] B.-G. Dong and H.-C. Guo, Chin. Phys. Lett. **21**, 2144 (2004).
[41] D. Rudolph *et al.*, Eur. Phys. J. A **4**, 115 (1999).
[42] C. E. Svensson *et al.*, Phys. Rev. Lett. **79**, 1233 (1997).
[43] C. E. Svensson *et al.*, Phys. Rev. Lett. **80**, 2558 (1998).
[44] A. Galindo-Uribarri, D. Ward, G. C. Ball, V. P. Janzen, D. C. Radford, I. Ragnarsson, and D. Headly, Phys. Lett. B **422**, 45 (1998).
[45] I. Ragnarsson, Acta Phys. Pol. B **27**, 33 (1996).